ARIANNE MAY JABONERO

DEPOSITION OF THICK NANOSTRUCTURED CR-BASED COATINGS BY HIPIMS

VOLUME 1

Dissertação no âmbito do Mestrado Conjunto Europeu em Tribologia de Superfícies e Interfaces orientada pelo Doutor Ricardo Gil Henriques Serra e apresentada ao Departamento de Engenharia Mecânica da Faculdade de Ciências e Tecnologia da Universidade de Coimbra.

Julho de 2021

1 2 9 0

FACULDADE DE CIÊNCIAS E TECNOLOGIA
UNIVERSIDADE D COIMBRA

Deposition of Thick Nanostructured Cr-based Coatings by HiPIMS

Submitted in Partial Fulfilment of the Requirements for the Degree of European Joint European Master in Tribology of Surfaces and Interfaces.

Deposição de revestimentos à base de Cr nanoestruturados espessos por HiPIMS

Author

Arianne May Jabonero

Advisor

Doutor Ricardo Gil Henriques Serra

Jury

President	**Professor Doutor Albano Augusto Cavaleiro Rodrigues de Carvalho** **Professor da Universidade de Coimbra**
Vowel	**Professor Doutor Ana Paula da Fonseca Piedade** **Professor Assistente da Universidade de Coimbra**
Advisor	**Doutor Ricardo Gil Henriques Serra** **Investigador da Universidade de Coimbra**

· U C ·

UNIVERSIDADE DE COIMBRA

tribos Joint European Master in Tribology of Surfaces and Interfaces

Ljubljana • Leeds • Coimbra • Luleå

Coimbra, Julho de 2021

ACKNOWLEDGEMENTS

The completion of this research project was made possible from the tremendous help provided by various individuals.

I am extending my heartfelt gratitude to my supervisor, Dr. Ricardo Serra, for incessantly providing unconditional support, valuable resources, prompt feedback, and all the necessary assistance needed for my work ever since the start of this academic year until the final stretch of this report. I am also thankful for the helpful comments and suggestions provided by Dr. Albano Cavaleiro, as well as his team in CEMMPRE, especially to Dr. João Carlos Oliveira, Dr. Fábio Ferreira, and Dr. Manuel Evaristo, who extended their time and effort amidst the restrictions during pandemic to help me in the entire deposition process and characterization of film coatings.

I also want to thank Instituto Pedro Nunes (IPN) for making the needed laboratory equipment available for the characterization of films.

Significant technical background on surface protection and tribology was also provided by Dr. Filipe Fernandes, Dr. Bruno Trindade, and Dr. Mitjan Kalin, for which had been proven valuable in understanding the essential concepts of this work.

I am also grateful for the moral support, helpful tips and advice shared between the whole batch of TRIBOS+ 2019-2021, as it made the past two years become bearable and memorable after all ups and downs that we surpassed together. We have grown and learned a lot from each other by embracing and understanding our cultural differences. All thanks to the program consortium as well for providing this opportunity that ignited our knowledge and interest in tribology.

Most of all, I am earnestly thankful to my parents, siblings, and fiancé who had been my constant source of strength and inspiration through their endless encouragement and motivation.

ABSTRACT

The fundamentals of film coatings have been continuously developed over the years as the demand for functional films are flourishing in the industries. Chromium film is one of the largely used material for decorative and surface protection purposes owing to its bright appearance and good mechanical properties. However, Cr films are found to be vulnerable to wear and abrasion especially when used in severe long-term conditions. Hence, this present work aims to deposit relatively thick Cr-based coatings (between 1 – 10 μm) with improved performance for increased life service. Deposition was carried out using HiPIMS, a magnetron sputtering technique known by producing highly ionized fluxes of sputtered material that results to dense films with excellent properties.

The first part of this work focused on investigating the deposition parameters that will result in denser film at varying values of peak current (I_p) having the same film thickness of approximately 1 μm. As the applied I_p increases, the deposition rate decreases but the film morphology becomes denser, and the columnar microstructures become unrecognizable. The second part of this work used the best performance conditions to deposit Cr films at increasing thicknesses by increasing the duration of deposition. The maximum film thickness obtained in this work reached to 10.3 μm deposited for 360 minutes. All deposition systems were performed using a Cyprium power supply from Zpulser^{TM} LLC, operated in DOMS mode.

A detailed study on the effect of film thickness to the film properties was performed through film characterization using Scanning Electron Microscopy, X-ray Diffraction, and Atomic Force Microscopy. Results showed a constant morphology of dense and compact film regardless of the thickness, all of which having a [110] preferential orientation without significant peak shifting. Meanwhile, the surface topography features have grown supported by the calculated grain size that also increases with film thickness. In effect, the surface height and roughness increase with film thickness, causing the film hardness to decrease as measured by Nanoindentation.

Other mechanical and tribological film properties were also evaluated using residual test measurement, linear scratch test and pin-on-disc test. The measured residual stress had no significant change with film thickness, unlike the elastic modulus of the film that increases as the film grows. The wear on the ball from the pin-on-disc test increases with thickness due to the increase in film roughness. However, the wear rate of the film decreases at increasing thickness mainly due to the increase of critical load resistance in the scratch test.

The deposited Cr films in this work show that the high ionization capacity of HiPIMS effectively maintained a dense microstructure even on thicker films. Moreover, film growth from continuous bombardment with Cr^+ ions generally resulted to changes of film properties that only have a gradual decrease in the mechanical film properties.

Keywords Chromium, PVD, HiPIMS, DOMS, thick coating, Cr film

RESUMO

O conhecimento fundamental sobre revestimentos tem sido continuamente desenvolvido ao longo dos anos, à medida que a procura por filmes funcionais aumentou por parte das indústrias. Revestimentos à base de crómio são materiais muito usados como revestimentos decorativos e para proteção da superfície graças à sua aparência brilhante e boas propriedades mecânicas. Contudo, os revestimentos à base de Cr são vulneráveis ao desgaste e abrasão especialmente quando usados em ambientes agressivos durante longos períodos de tempo. Assim, o presente trabalho pretende obter revestimentos à base de Cr relativamente espessos (entre 1 – 10 μm) com boa performance para longos tempos de serviço. Os filmes foram preparados por HiPIMS, uma técnica de pulverização catódica conhecida por produzir fluxos de material com elevada fração ionizada o que resulta em filmes densos e com excelentes propriedades.

A primeira parte do trabalho focou a investigação dos parâmetros de deposição que originam filmes densos para variados valores de corrente de pico (I_p) com espessura até 1 mm. Com aumento do Ip a taxa de deposição diminui, a morfologia do filme torna-se mais densa e com estrutura colunar pouco percetível. A segunda parte deste trabalho usou então as condições que apresentaram melhores propriedades para depositar filmes Cr com maiores espessuras através do aumento do tempo de deposição. A maior espessura obtida foi cerca de 10,3 μm para 360 minutos de deposição. Todas as deposições efetuadas neste trabalho usaram uma fonte Cyprium da Zpulser™ LLC, operada em modo DOMS.

Um estudo detalhado do efeito da espessura nas propriedades dos filmes foi efetuado caracterizando-os com microscopia de varrimento eletrónico, difração de raio-X e microscopia de força atómica. Os resultados mostram uma morfologia densa e compacta constante independentemente da espessura e uma orientação preferencial [110] sem grandes desvios nos picos. Por outro lado, observou-se crescimento das partículas da superfície, sendo este resultado suportado pelo aumento do tamanho de grão calculado com aumento da espessura. A rugosidade e altura das partículas da superfície também aumentam com a espessura, levando a uma diminuição da dureza do filme medida por Nano-indentação.

Outras propriedades mecânicas e tribológicas dos filmes foram obtidas com medição das tensões residuais, teste de indentação deslizante e pino-disco. As tensões residuais não apresentam variação significativa com aumento da espessura, ao contrário do modulo elástico do filme que aumenta com o aumento da espessura. Já o desgaste na bola durante ensaios pino-disco aumentou com a espessura devido ao aumento da rugosidade superficial. No entanto, a taxa de desgaste do filme diminui para maiores espessuras principalmente devido ao aumento da carga critica, conforme verificado no ensaio deslizante.

Os revestimentos à base de crómio deste trabalho mostram que a elevada capacidade de ionização do HiPIMS permite manter uma microestrutura densa mesmo em revestimentos espessos. Mais, o crescimento dos revestimentos a partir de bombardeamento constante com iões Cr^+ resulta em modificação das propriedades do filme que apresentam apenas uma diminuição gradual nas suas propriedades mecânicas.

Palavras-chave Cromo, PVD, HiPIMS, DOMS, revestimento espesso, filme de Cr

CONTENTS

LIST OF FIGURES

LIST OF TABLES

SYMBOLS AND ACRONYMS

Symbols

$a_{(110)}$	Lattice parameter of (110) diffraction peak
Ar	Argon
Ar^+	Argon ion
Cr	Chromium
Cr^+	Chromium ion
CrN	Chromium Nitride
D	Pulse duration
DC_{int}	Internal DC power supply
F	Pulse frequency
I	Current
I_p	Peak current
L_c	Critical load
P	Pressure
P_a	Average power
P_p	Peak power
Ra	Surface roughness
Rz	Height of surface features
Si	Silicon
T	Oscillation period
Ta	Tantalum
t_{dep}	Deposition time
TiO_2	Titanium dioxide
T_m	melting temperature
t_{on}	Oscillations ON time
V	Voltage
V_p	Peak voltage

Acronyms

AC	Alternating current
AFM	Atomic Force Microscopy
BCC	Body centered cubic
CAD	Cathodic Arc Deposition
CEMMPRE	Centre for Mechanical Engineering, Materials and Processes
COF	Coefficient of friction
CVD	Chemical Vapor Deposition
DC	Direct current
DCMS	Direct Current Magnetron Sputtering
DOMS	Deep Oscillation Magnetron Sputtering
EHD	Electrohydrodynamic
ESZM	Extended Structure Zone Model
EU	European Union
FWHM	Full width at half maximum
HiPIMS	High Power Impulse Magnetron Sputtering
HPPMS	High Power Pulsed Magnetron Sputtering
ICDD	The International Centre for Diffraction Data
MPPMS	Modulated Pulse Power Magnetron Sputtering
OM	Optical Microscopy
OSHA	Occupational Safety and Health Administration
PVD	Physical Vapor Deposition
REACH	Registration, Evaluation, Authorization and Restriction of Chemical substances
RF	Radio frequency
RFMS	Radio Frequency Magnetron Sputtering
RoHS	Restriction of Hazardous Substances Directive
SCCM	Standard Cubic Centimeters per Minute
SEM	Scanning Electron Microscopy
SZM	Structure Zone Model
XRD	X-ray Diffraction

1. INTRODUCTION

1.1. Motivation

Film coating is primarily composed of material layer(s) having a thickness ranging from fractions of nanometer to several micrometers. It has diverse technological and industrial applications owing to the enhanced properties of applied component as a combined effect of thin film protection and improvement of the surface on top of the existing properties of bulk material. Application of films on surfaces are referred to as deposition process. The first widespread deposition technique was discovered in the early 1800s by Italian chemist Luigi V. Brugnatelli [1] through a process called electroplating. Due to the low quality of resulting film coating, another deposition technique was then developed by W.R. Grove in 1852 to what is now known as sputtering [2] which will be discussed in detail in Section 2.3.2.

The demand for functional films has increased over the years as research works related to the fundamentals and technical aspects of film coatings are continuously developed. Among the widely used film materials is Chromium (Cr) due to its notable hardness and wear resistance hence commonly used for surface protection [3,4] and decorative applications [5]. However, when used in severe long-term conditions, Cr coatings are found to be vulnerable to corrosion and abrasion that eventually leads to surface degradation and material failure [6,7]. With this, deposition of Cr films was sought to be applied at a higher thickness to improve the coating performance and increase the life service. Several deposition processes were already investigated in obtaining thick Cr films to meet various engineering applications.

Electroplating is one of the commonly used deposition technique of Cr films, yet results exhibited coatings with low density, poor adhesion, as well as the recently posed health and safety risks (see Section 2.2). Some studies also obtained thicker Cr coatings (greater than 20 μm) using plasma spraying [8] and cathodic arc deposition (CAD) [9] but the resulting coatings are either porous, or uneven surface with high surface roughness. Magnetron sputtering is also one of the deposition techniques explored in this film application that was able to provide uniform coatings, with high density and adhesive properties [10,11]. This

technique is categorized under Physical Vapor Deposition (PVD) process that involves ionization of atoms and interaction with source material causing atoms to be ejected or sputtered to the substrate where it condenses to form a film coating [12]. Its mechanism allows deposition of films even at low substrate temperature and more control on the parameters, thus film structure and properties can be further optimized.

High-Power Impulse Magnetron Sputtering (HiPIMS) is one of the recently developed variation of Physical Vapor Deposition (PVD) techniques in the last decades that is known to produce high ionization degree of source material resulting in much denser films with excellent properties. More details on the mechanism of this technique are discussed in Section 2.4.1. However, this deposition process is found to have considerably lower deposition rate compared to other sputtering techniques [13-15] making it one of its major drawbacks. Given the superior film coating quality produced by HiPIMS and all its other advantages, part of the motivation of this research work is to gain an in-depth understanding of film characteristics in relation to its growth.

This research project mainly aims to explore the deposition of relatively thick film (more than 1 μm) made from pure Cr using HiPIMS system and investigate the effects on film characteristics. Deposited films will be characterized using X-ray Diffraction (XRD), Scanning Electron Microscopy (SEM), hardness test, and pin-on-disk wear test, among others, in an effort to correlate the film microstructure, morphology, residual stress, mechanical and tribological properties, with the thickness of deposited film.

1.2. Objectives

This master thesis project aims to develop a relatively thicker Chromium film to be deposited on a substrate using HiPIMS while maintaining the high density and good mechanical properties. The main objective can be achieved by performing the following:

i. Confirmation of deposition parameters that will result to a highly dense film using previous related studies of the same target and deposition technique;

ii. Analysis of varying film thicknesses and correlate with the structural and morphological film properties using different material characterization techniques;
iii. Investigation on the influence of film growth to the mechanical and tribological properties through various related tests such as scratch test, hardness test, pin-on-disc, and other tests.

1.3. Thesis Structure

The research project entitled "Deposition of Thick Nanostructured Cr-based Coatings by HiPIMS" is accomplished as a master thesis project that forms part of the completion requirement on the master program Joint European Masters in Tribology of Surfaces and Interfaces. This project aims to deposit a thick Cr film coating on a substrate using HiPIMS technique.

The objectives and structure of the master thesis are defined in Section 1. Meanwhile, the background and related literatures of the topic are outlined in Section 2 under State of the Art, discussing the deposition process of thin film coating, Cr deposition, PVD process, sputtering effects, and characteristics and challenges in depositing thick Cr films using HiPIMS. Section 3 specifies the materials to be used and the experimental procedure, while the experimental results are thoroughly discussed in Section 4. The conclusion of the project and recommendations for future studies are listed in detail under Section 5.

2. STATE OF THE ART

This chapter provides some relevant background information related to the subject matter being studied such as thin film coatings, Cr-based films, deposition processes specifically PVD, and more in-depth overview on thick Cr-based films using HiPIMS.

2.1 Thin Film Coating

A layer of material with a thickness that ranges from fractions of nanometer to several micrometers is referred to as a thin film. It can be synthesized to be a composition of single or multiple elements, phases, layers, resulting to homogenous or composite microstructures depending on the intended purpose. Categorized under the umbrella of coating materials, thin films are mainly applied on a material surface or substrate in order to improve the substrate performance or modify the surface properties and morphology without affecting the bulk properties.

With the premise that thin film materials can be synthesized in a controlled manner, it became an integral part of research and industrial processes over time. Its applications have also reached a wider scope such as in tools and equipment that require improvement on surface properties like corrosion, fatigue, hardness, and wear. Advanced technologies also utilize thin film for various reasons making it a versatile coating for superconducting machines and cables [16], semiconductor [17], electronic and magnetic devices [18], hard and optical coatings [19,20], energy storage and generation [21,22].

2.1.1. Deposition Process

The application of thin films onto a surface is generally called deposition. In some cases, it is particularly called atomistic deposition as it involves individual atoms of molecules being deposited either on a bare substrate surface or on top of a previously deposited layer. The

process of atomistic deposition can be classified into three main categories – electrolytic deposition, chemical vapor deposition (CVD), and physical vapor deposition (PVD).

One of the advanced forms of electrodeposition is the electrohydrodynamic (EHD) deposition or electrospray that uses a nanoparticle solution as a source material being fed to a capillary nozzle that is connected to a high voltage [23]. When current is applied through the system, a jet of thin film made of fine positively-charge droplets spurts from the nozzle then uniformly deposited on the substrate. Some other processes that are more known to be functioning in an electrolytic environment are electroplating, electrophoresis, and autocatalytic or electroless plating.

A thin film deposition process that utilizes the chemical vapor environment generally refers to CVD and its different variations such as Laser CVD, Plasma Assisted CVD, Atomic Layer CVD, etc. CVD occurs in a reaction chamber that involves the chemical reactions of one or more volatile materials, often called as precursor gas, on the heated substrate surface resulting to thin film deposition [24]. The chemical by-products produced from the reaction are then removed from the chamber by a gas flow process together with the unreacted precursor gases.

The process of thin film deposition using a physical vapor is called PVD. This type of deposition process basically involves the transformation of source material from solid or liquid, to vapor phase, through a plasma environment, or low pressure gaseous or vacuum environment to the substrate. The vapor then goes back to solid phase after it condenses as a thin film on the substrate. It comprises the largest group of gas-phase and plasma-based coating processes, hence PVD process is primarily divided between Evaporation (gas-phase) and Sputtering (plasma-based) techniques [25]. More details on these processes will be provided in Section 2.3.

Main difference between CVD and PVD is the applicability of thin film materials wherein CVD is more selective as it requires chemical reaction, while PVD has less restriction on the target materials. Meanwhile, CVD is mostly preferred for commercial thin-film deposition technique as it is relatively cheaper than PVD with higher deposition rate. However, PVD is known to generate thin films with excellent adhesion on most materials with more control on the applied chemical and physical parameters of source materials.

2.1.2. Film Materials

Part of the versatility of thin film deposition is the wide range of material choices that can be applied on a substrate depending on the intended purpose. This source material is commonly referred as the target material especially in PVD techniques, which is being ejected from energized ions or (inert) gas onto a substrate. Ejected atoms from the target material have a wide range of energy, reaching up to tens of electron volts (eV) [23].

Target materials are one of the essential deposition components, along with the parameters, as it physically translates to the resulting thin film material [26]. These materials are generally outsourced commercially, and comes in varying shape, size, and composition. It can be made from alloy, compounds, or pure metals.

Alloy targets can be further categorized either as magnetic, non-magnetic, noble metallic, or suitable for high temperature services. Target materials can also be made of compounds or mixture of elements such as oxides, carbides, nitrides, phosphides, or sulfides. It can also be sourced out from pure metals such as Aluminium, Cobalt, Copper, Iron, Magnesium, Manganese, Tin, and Chromium.

2.2 Chromium Films

Grouped under pure metal target material, thin films that are based on Cr are found to be useful in a wide variety of applications due to its excellent performance with good tribological properties. Chrome coatings are known to have high hardness and low coefficient of friction hence it is extensively used on components that require wear and abrasion resistance. Some of its applications include hard coatings for cutting-edge materials [27], industrial components like machining tool and wear parts [28], aircrafts [29], automotive [30], nanomaterials [31], electronics [32], magnetic and optical devices [33], and materials in energy industries [34].

One of the well-established deposition processes having the most available historical data in this type of film is the hard chrome plating. While prominent for its effectivity, affordability, and excellent wear properties, usage of chrome coating also possesses some drawbacks such as low deposition rates due to the low electrolytic efficiency, and formation of toxic hexavalent Cr ions leading to health and safety risks.

Chromium is highly dependent on oxidation state and in order for the plating deposition mechanism to be highly effective, the reaction shall result to a strong oxidizing agent in the form of hexavalent Cr or Cr(VI). However, substantial evidences [35] have found showing the carcinogenicity of Cr(VI) compounds which are commonly traced from chrome plating industries. Studies have also shown that long exposure to these compounds result to various respiratory diseases, skin irritation, and kidney damage [36].

With its adverse effects on the health and safety, a ruling related to the controlled exposure and reduction of permissible exposure limit on Cr(VI) compounds had been implemented by the US Department of Labor's Occupational Safety and Health Administration (OSHA) since May 30, 2006 [37]. Directive 2011/65/EU also entered into force last July 21, 2011 restricting Cr(VI) concentration on electrical and electronic equipment for up to a maximum of 0.1% as per of EU RoHS (Restriction of Hazardous Substances Directive) 2 [38]. The most recent regulation took effect since September 21, 2017 where usage of Cr(VI) has been totally prohibited in Europe under the revised Appendix XIV of Registration, Evaluation, Authorization and Restriction of Chemical substances (REACH) [39].

Given the imposed restrictions of Cr(VI) as a result of hard chrome plating, other alternative deposition techniques of Cr material have been developed such as cold spraying [40], thermal spraying [41], flame spraying [42], sputtering [43], ion implantation [44], and trivalent chromium plating [45]. These processes resulted to various degree of coating properties and deposition parameters thus understanding the related behavior, properties, and microstructure of the deposited films remains rare with limited related literatures.

2.3 PVD Process

The deposition process that involves physical coating of thin film onto a surface is commonly called Physical Vapor Deposition (PVD). This technique entails the growth of coating through physical discharge of atoms or molecules on the substrate when the vaporized source material called target condenses on the surface under certain conditions. Several deposition techniques are classified under PVD and it can be generally grouped based on the type of environment that the process works on. The most common PVD processes are Evaporation and Sputtering which both allows the deposition of particles from the target to the substrate using a reactor shown in Fig. 2.1, comprising a vacuum chamber and electrodes that are connected to a power supply.

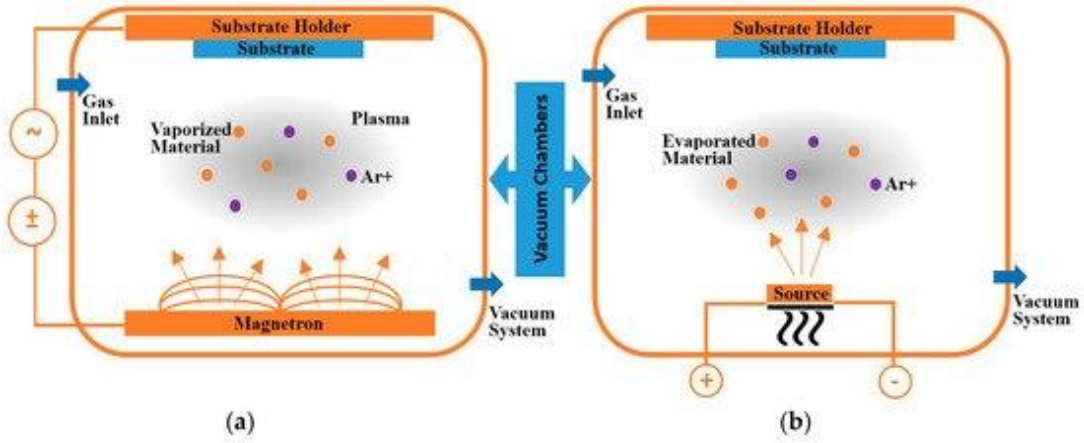

Figure 2.1. Schematic drawing of two conventional PVD processes: (a) sputtering and (b) evaporating using ionized Argon (Ar^+) gas [25].

2.3.1. Evaporation

Evaporation is a simple form of PVD that utilizes heat or thermal energy on the source material until it reaches its vaporization point which then condenses on the substrate to form the film coating [26]. There are several methods in heating the source such as hot filament, electron beam, electrical resistance, and cathodic arc. This process works in a chamber with high vapor pressure resulting to a higher deposition rate compared with sputtering. However, since this process is mainly dependent on the evaporation process of material from the heat source, the film thickness and dispersion of particles cannot be controlled. As an effect, deposited films have lower adhesion and lacks homogeneity.

2.3.2. Sputtering

Sputtering is a PVD technique based on the bombardment with energized ions, usually from an inert gas, that causes the atoms from the target material to be sputtered and deposited on the substrate. The ions can be produced by either directly from an ion source or a plasma. The former is straightforward sputtering from the ion source to the target but is often utilized for surface analytical techniques only, as the bombardment area is only limited, and the deposition rate is relatively low. Meanwhile, the latter is found to be more suitable on film deposition at a larger scale. Plasma is produced when a power source is introduced to the target with electrical discharge coming from a gas medium (i.e., Argon) resulting to energized ions in the electric field upon the application of high voltage. Attraction then occurs from the positively charged ions in the plasma towards the target receiving sufficient energy to bombard the target and initiate material sputtering. Electron movement in this system is defined by the electrical field between the cathode and the anode. This typically requires operation at a relatively high pressure, i.e., of the order of a few Pa, for the electrons to produce sufficient ions in order to sustain sputtering.[46]

In its basic form, a sputtering system is comprised with a vacuum chamber, metallic anode and cathode, energized by a voltage in several keV and pressure of more than 0.1 Pa in order to obtain a glow discharge of plasma [46]. The process mainly depends on ion bombardment hence the atomic weight of the discharge gas shall be almost equivalent to the target material in order for the momentum energy transfer to be optimized. Ejected atoms from the cathode or target material disperses going to the anode which is the substrate where thin film is formed. Deposition process can be done either in a vacuum or gas environment where plasma is generated. In addition to the physical process of sputtering, chemical reaction may also be applied by introducing reactive gas on the vapor which is called as reactive sputtering.

The method of sputtering depends on the target configuration or how it functions to deposit the thin films such as through magnetron, ion beams, diodes, or triodes. Magnetron is one of the most common sputtering sources that utilizes strong magnetic fields in restricting the charged plasma particles close to the target surface in order to increase the efficiency of electron confinement. This technique tends to elongate the electron trajectory thus allowing an optimal movement of the ions and sputtered atoms to the substrate even with a reduced voltage

and discharge pressure [46]. This results in the production of more gas ions for the same electron density thus increasing the rate of deposition. Some general features of magnetrons to be considered in sputtering are the discharge voltage, discharge current and its behavior with the voltage, magnet configuration – planar or rotating, and applied power. Sputtering techniques under magnetron can be further categorized based on the applied power supply which can be either direct current (DC), alternating current (AC), or radio frequency (RF). One of the more recent sputtering technique is the high-power impulse magnetron sputtering (HiPIMS) that uses a large energy pulse over a very short period, typically around 100 μs.

Having a wider variety of deposition process based on the target material and source configuration, sputtering allows more control on the desired thickness of deposited film ranging from few nanometers to very thick layers of coating deposition. It also allows more adjustment on the deposition parameters and deposition duration leading to a more homogenous and adhesive film. However, presence of contaminants on the surface is one of the typical problems in this deposition type due to the desorption of particles in a plasma-based sputtering. More advantages and limitations of sputtering will be discussed in Section 2.4.

With the ability to control the film properties such as crystalline structure, roughness, and morphology, sputtering technique is usually used to deposit oxide and metallic films for microelectronics and semiconductor devices. Some other applications also include optical coatings, nanomaterials, lubricant films, tool coating, and decorative applications.

2.4 Deposition of Cr Films using HiPIMS

2.4.1. HiPIMS

The quality of deposited films can be further optimized in terms of density, applied parameters, and resulting film properties using more advanced sputtering techniques such as HiPIMS. As the name suggests, it utilizes a high-power impulse to increase the ionization process of the sputtered material in the plasma. It is then generally categorized as an ionized PVD process derived from the conventional DCMS. In principle, increasing the power results to an increase in the plasma density thus more ionization of sputtered material is obtained. This

also increases ion bombardment in the target, where significant part of their energy is transformed into heat energy. In order to control the temperature at the target, high power is repeatedly applied in short pulses, thus calling the process an impulse magnetron sputtering. In this manner, the target temperature is kept below its melting point as the time average power is maintained low allowing the system to cool down.

The typical pulse of a discharge by an operation variant of HiPIMS, deep oscillation magnetron sputtering (DOMS), is shown in the voltage-current plot of Fig. 2.2. Generating large energy impulse requires high peak voltages, typically around 500 – 1500 V, current density of few A/cm^2 as per sample references [13-15], and high peak power densities, about 1 – 3 kW/cm^2, versus conventional magnetron sputtering with a range of 1 – 10 W/cm^2 power density [46]. A low average power within few W/cm^2 is maintained using a time average power ranging from 10 – 1000 μs [47,48]. Meanwhile, the shape of discharge pulse also varies depending on the load being formed as well as the type and pressure of gas used.

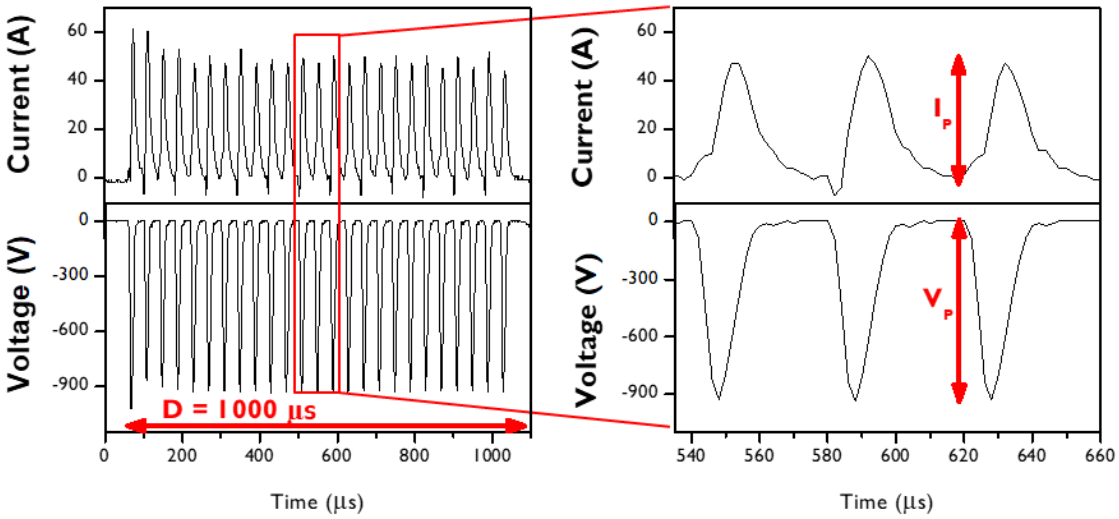

Figure 2.2. Voltage-current waveforms of a HiPIMS pulse in DOMS mode at a pulse duration (D) of 1000 μs marked with maximum current (I_p) and voltage (V_p) for each oscillation.

Several literatures [47-50] explained the behavior of plasma in thin film deposition and the different plasma discharge regimes created depending on the applied current and voltage. In theory, sputtering takes place at a plasma density ranging from 10^{15} – 10^{19} m^{-3} referring to the density of resulting charge carriers from ionization. In HiPIMS system, the high power and high voltage being applied causes a tremendous increase of charge carriers thus also increasing the electron density in the ionization region near the target surface to ~ 10^{19} m^{-3}.

With such order of electron density in the discharge, a significant fraction of the sputtered material has the possibility to be ionized making it a fundamental feature of HiPIMS.

2.4.2. Film Characteristics

Given the large flux of ionized sputtered material from HiPIMS, the resulting thin films are generally denser than other techniques due to the reduced film porosity brought by the ion flux that is said to enhance surface mobility of adatoms [51]. The high degree of ionization of the sputtered species can also be utilized in pre-cleaning of substrate surface prior deposition by sputtering away some existing contaminants and oxide layers. Due to ion bombardment during surface pretreatment, some ions have the tendency to be implanted on the substrate creating a composition change from the substrate to the deposited film. Some studies found that this type of pretreatment helps in the improvement of surface adhesion [52] as well as the enhancement of surface properties such as wear and corrosion resistance [53]. The ion energy from HiPIMS discharges can also be measured resulting to an average energy of approximately 20 eV [54]. Thin films produced with ion energies between 20 – 30 eV were found to be denser [55].

HiPIMS can also have various effect on the growth and properties of thin films. One of which is the possibility of deposition on complex-shaped substrates with the aid of substrate bias where negative voltage is applied to attract and specify the direction of the ionized material. This has been successfully applied in film deposition on the sidewall of a trench for semiconductors with the aid of substrate bias, electric and magnetic fields in guiding the ionized materials [56,57].

The phase compositions of thin films can also be altered by varying the deposition parameters in terms of kinetic and thermodynamic conditions. This was demonstrated in Ta film deposition at a controlled magnitude of internal stress resulting to higher ionization flux on the surface compared with DCMS [58]. The efficiency of momentum transfer in such case was due to the high ionization degree of Ta vapor that generally reaches up to 70%. Another example is the control of TiO_2 phase, that can grow either in rutile or anatase phase, with the addition of reactive gas in the HiPIMS system [59]. Rutile phase is said to be normally formed

at high temperatures [60], but due to the flux increase of ionized species, formation of rutile phase is favored than anatase phase even at room temperature [59].

Film microstructure can also be controlled using HiPIMS thereby allowing the morphology, mechanical strength, and other film properties to be optimized. One factor that affects the microstructure is the deposition temperature wherein sputtering at temperature lower than $0.4T_m$ (melting temperature of the target material) leads to formation of highly porous columnar microstructure [61]. A study on the deposition of CrN film [61] showed that increasing the peak target current of HiPIMS resulted to repeated nucleation causing the suppression of the columnar structure and transition of morphology from dense polycrystalline to featureless nanocrystalline. This result was due to the increase of ion flux to the substrate with relatively low energies as discussed in Section 2.4.2. The deposited CrN film was said to have higher hardness, lower coefficient of friction, and enhanced tribological properties as compared to the films deposited by DCMS [62]. The same improvement of properties, including the increase of adhesion strength and decrease of residual stress, was also demonstrated in the deposition of CrN_x film using HiPIMS [53].

2.4.3. Sputtering Effects

Bombardment with energized particles has several effects within the surface region of the substrate. As illustrated in Fig. 2.3, bombarding particles move differently on the surface, near the surface, or below the surface depending on the effects brought by cascading collision and momentum transfer. Collision of atoms in vacuum sputtering, such as in HiPIMS, involves high energy sputtered atoms and high energy reflected neutrals of the bombarding gas, both greatly affects the process of film deposition.

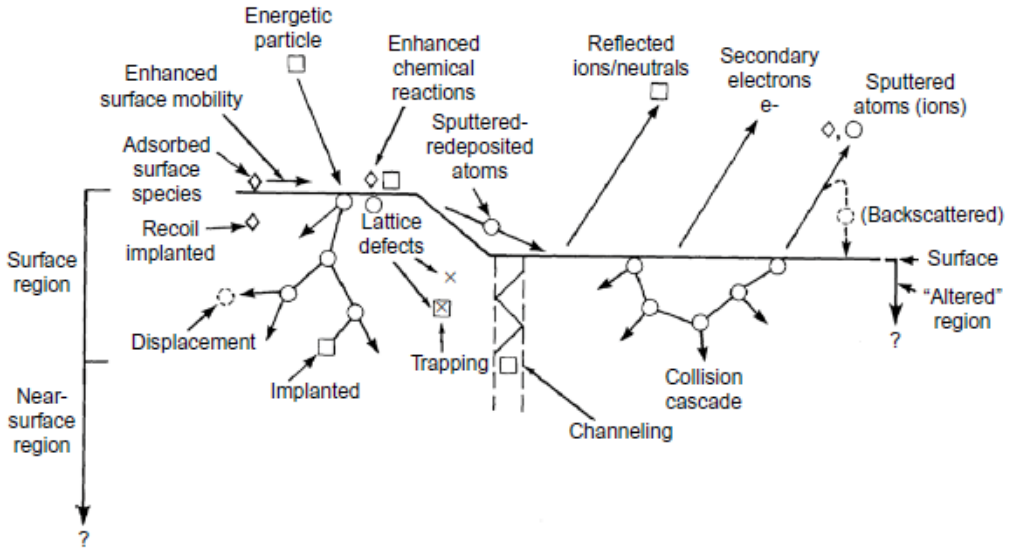

Figure 2.3. Particle movements in the surface region bombarded with energized atomic-sized particles [63].

One of the bombardment effects in the substrate is *re-sputtering* of deposited material mainly caused by the high energy of particles impinging on the growing film that exceeds the sputtering threshold of target material. The energetic bombardment of neutral film may cause residual stress on film growth that consequently causes dislocation on the surface [63]. Another substrate-related occurrence is the preferential growth of atoms forming hills on the surface, which is called *shadowing effect*. This contributes to under dense regions, typically valleys or surfaces that are not perpendicular with the incident deposition flux, resulting to formation of columnar microstructure [64,65]. Deposition at higher bombardment energy however reduces the formation of atomic shadowing.

Target materials can also have considerable effects on the sputtering process. There are cases when the energetic ions of the target material are the same particles bombarded back to the target causing *self-sputtering*. This consequently results to a reduction of sputtered particles reaching the substrate as the newly formed ions from sputtered atoms return to the target [66]. It can also be related to another effect called *return* and *yield* wherein the former occurs when the metallic ions are attracted back to the target instead of depositing to the substrate, while the latter refers to the loss of sputtering efficiency at higher voltages [65]. Deposition at high target voltages also results to higher ionization rate of sputtered atoms and increased probability of ions returning back to the target due to the increased ion retarding potential in the target area [67]. Both effects prevail at high peak power as they are influenced

by the peak current and peak voltage, typically used in HiPIMS [68]. All these effects are known to decrease the deposition rate as presented in several related studies [13,14,65,66].

The applied deposition parameters of sputtering also play a significant role on the deposited films, especially its microstructure and morphology. The fundamentals of this reaction process are commonly explained by several researchers using the classic structure zone model (SZM) published by Thornton [69]. Mahieu et. al. recently developed this model [70] by also investigating the insights of thin film growth, other than the microstructure, as influenced by the deposition parameters. Figure 2.4 shows the summarized schematic structure of the extended structure zone model (ESZM).

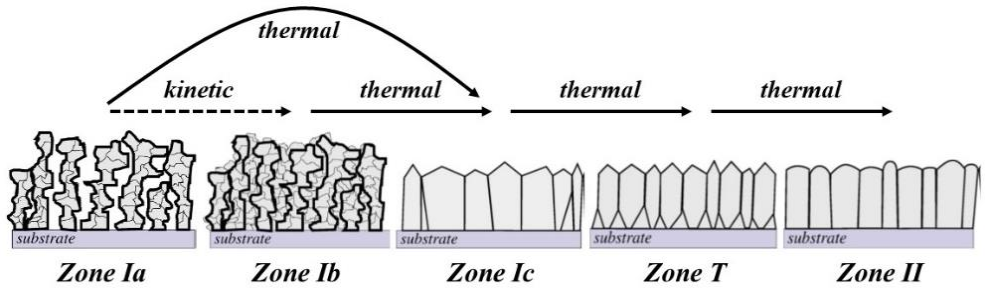

Figure 2.4. Overview of schematic structures based on transition energy per identified zones in the ESZM [70].

The schematic structures show that microstructures evolve as a function of adatom mobility depending on the energy flux per sputtered particle as an effect of deposition parameters [70]. Zones *Ia* and *Ib* both have no mobility and preferential orientation, with shadowing that influences the growth and columnar structure. The only difference is that Zone *Ia* has voids while Zone *Ib* are separated by grain boundaries. Surface diffusion with polycrystalline structure was observed from Zone *Ic* onwards, but growth is still caused by shadowing in this zone and still has no preferential orientation. Crystal growth can be observed from Zone *T* to Zone *II* resulting to increase in film thickness and change in microstructure showing preferential orientation and columns from V-shaped to straight. Zone *II* has the highest temperature that causes recrystallization and restructuring leading to oriented columns with planes of lowest surface energy due to thermodynamic stability.

2.4.4. Thick Cr Deposition

The distinct properties of Cr films as discussed in Section 2.2 can be further improved to be more cost effective by increasing the coating performance at a higher life service. This can be achieved through the application of a relatively thick coating, approximately more than 5 μm, which also requires a higher deposition rate.

However, HiPIMS is known to have a lower deposition rate compared to other sputtering techniques with the same average power, like DCMS [13], thus posing a challenge in the deposition of thicker films. This may also be the reason why there are only very limited studies [71,72] related to thick Cr deposition using HiPIMS. Some of the causes for the reduction of deposition rate were already discussed in the previous section.

Considering that HiPIMS technique develops film coatings with high density, good adhesion, excellent mechanical and tribological properties, deposition of relatively thicker Cr films will still be explored using more controlled deposition parameters. Previous works that obtained Cr films with excellent structure and properties [66,68] will be used as a benchmark for the parameters to be applied, specifically peak current and peak power. Deposited film thickness will be gradually increased with deposition time while subsequently checking the film properties using surface characterization techniques so as not to compromise the quality of coating over thickness.

If successfully developed, this type of coating can be useful for components that will be utilized in severe operating conditions at extended duration. Some applications that require superior mechanical properties for a longer period include cutting tools and die moulds in large-scale industries.

3. EXPERIMENTAL PROCEDURE

3.1 Deposition of Films

The Chromium (Cr) films were deposited from a high purity (99.98%) Cr target material onto silicon (Si) wafers (100) and high-speed steel (M2) samples polished until mirror-like surface was achieved. All substrates were ultrasonically cleaned in acetone and alcohol prior to the depositions. They were fixed to a rotating substrate holder that revolved at 25 rpm around the central axis of the chamber that is 80-mm away from the target material. The flow rate of applied inert gas, argon, was kept constant at 20 sccm for all depositions, with working pressure set to 0.5 Pa in all depositions. The deposition process was carried out using HiPIMS in DOMS mode via Cyprium^{TM} III plasma generator (Zpulser Inc.) that is continuously operated by an internal DC (DC_{int}) power source.

A typical example of the discharge voltage and current in HiPIMS was discussed in section 2.4.1. Each pulse (D) in Fig. 2.2 is comprised of several sequential single oscillations, with voltage and current that gradually increases during on-time (t_{on}) until they reach the maximum values (V_p and I_p), then gradually decays up to zero before the end of oscillation period (T). Depositions were performed at a constant D, t_{on}, and T having the respective values of 1000, 6, and 40 μs. The pulse frequency (F) was automatically adjusted by the DOMS power supply software to maintain a constant average power (P_a) of 1.2 kW. In this work, the peak power (P_p) is identified as the product of average maximum values of V_p and I_p for each oscillation.

Before all depositions, a base pressure below 5 x 10^{-3} Pa was reached inside the deposition chamber. An Ar plasma etching process was also performed to improve film adhesion through initial heating of the target and further cleaning of both the target and substrate surface against impurities. This process was performed for 10 minutes using DOMS power supply and HiPIMS pulser (HiPSTER ENI) at 700 V (600 Hz and 100 μs reverse time), generating 8 W of power and 0.01 A of current on the substrate holder. A shutter plate was

placed between the substrate and target material to prevent the sputtered Cr species from reaching the substrate during the etching process.

Two series of depositions were performed in this study having different conditions. The first series of Cr films aimed the identification of the deposition parameters that will result in dense film through all their thickness. In this regard, the deposition was done with different peak currents (I_p) through gradual increase of the charging voltage (DC_{int}) of HiPIMS power supply from 300 V to 400 V. Deposition times have been adjusted to maintain an average coating thickness of approximately 1 - 1.5 μm in all samples for this series. All other deposition parameters were kept constant. To further investigate the bombarding effect on growing films, the chosen I_p in the first series was then utilized in the second series of Cr films. At a constant value of I_p, the deposition time was doubled in each sample for the purpose of increasing the deposited film thickness. The recorded thicknesses along with the summary of applied deposition parameters are listed in Table 1.

3.2 Characterization of Films

Film thickness and morphology were measured using scanning electron microscopy (Quanta 400FEG ESEM) with 2 keV beam to acquire micrographs in several surface and cross-sectional areas of Cr films at similar amplifications.

Analysis of film microstructure was performed through X-ray diffraction (PANanalytical X'Pert PRO MPD) in θ–2θ geometry of parallel beam using Cu Kα radiation (45 kV and 40 mA). The XRD equipment was mounted with parallel plate collimator (0.7°) and Soller slits (0.004°) on the path of the diffracted beam, and a hybrid monochromator (with a Cu W/Si mirror and a double crystal Ge (220)) on the incident beam optics. X-rays were collected using a PIXcel detector in receiving slit mode. The films were scanned from 30° to 140° (except 69° to 71°) to avoid the (111) diffraction peak of the Si substrate. The recorded XRD spectra were fitted using a pseudo-Voigt function to obtain the corresponding values of peak position (2θ) and full width at half maximum (FWHM). Calculation of grain size was done using Scherrer's equation, while the lattice parameter was obtained using Bragg's equation and the geometrical relationship equation of lattice parameters with Miller indices and interplanar distance.

The roughness and topography of films deposited on Si wafer were investigated using Bruker Innova atomic force microscopy (AFM) in contact mode. Applied cantilever is made of silicon material with a nominal tip radius of 6 nm at a frequency of 300 KHz. Multiple 2 x 2 μm areas were scanned on each film to ensure proper representation of the sample surface. The statistical quantities were obtained from the AFM scans using the Gwyddion software (version 2.58) after leveling the surface.

3.3 Mechanical Film Properties

The residual stress induced on the Cr films was measured based on the resulting curvature after film deposition. Measurement of curvature radii of all films was obtained using an optical profiler (Mitutuyo Surftest SJ-500) in two orthogonal directions along the x and y axes. Average values of measured radius per sample were recorded to calculate the internal stresses of deposited films using the Stoney equation [73].

Evaluation of film adhesion behavior was done using an instrumented linear scratch test (Swiss CSEM) with a Rockwell C indenter having a tip radius of 200 μm and conical angle of 120°. The scratch test was applied on Cr films deposited on AISI M2 steel substrates. Application of load was linearly increased from 3 N to 70 N creating a scratch length of 7 mm on the film. The obtained scratch tracks were examined by optical microscopy (OM) using a Leica DM4 B vertical microscope to evaluate the critical load and assess the mode of coating failure.

Film hardness and Young's Modulus were obtained by nano-indentation technique (Micro Materials NanoTest) using a Berkovich diamond pyramid indenter. Evaluation of hardness was performed from load-displacement curve using the depth-sensing mode. Hardness measurements were done with 5, 10, and 20 mN loads (16 measurements for each load) in order to evaluate possible influences of the substrate and/or indenter size effects. To keep the indentation depth to less than 10% of the thinnest film, only the recorded values from 10 mN applied load were selected to be presented in this work. The hardness values at such load agreed well within the experimental error.

The tribological properties of deposited films were examined using a homemade pin-on-disc set-up as shown in Fig. 3.1 in an ambient air atmosphere (temperature of 22±1°C and relative humidity of 48±1%) without a lubricant. The disc material is made of AISI M2 steel where Cr films were deposited, while the sliding counterpart if made of AISI 52100 ball with a diameter of 10 mm. All tests were performed with a normal load of 1 N, sliding speed of 0.1 m/s, and duration of 20,000 cycles resulting to a total distance of 754 m. The average coefficient of friction (COF) was continuously acquired during the test using a load-cell and the results at the steady sliding state have been recorded. Wear tracks on the discs were studied using a surface profilometer (Mitutuyo Surftest SJ-500) to measure the volume loss due to wear (mm^3) and calculate the specific wear rate (mm^3/Nm) in accordance with Archard's law [74].

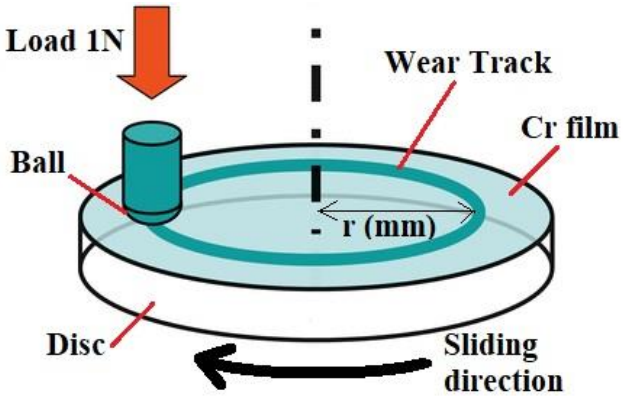

Figure 3.1. Pin on disc set-up used for tribological test of Cr deposited films.

4. RESULTS AND DISCUSSION

4.1 Deposition of Films

Two series of depositions were performed in this research work. The applied deposition parameters and resulting thicknesses of deposited thin films are shown in Table 1. The deposition chamber pressure was kept constant at 0.5 Pa, as well as the average power (P_a) at 1.2 kW by controlling the frequency of HiPIMS pulses from 207 to 113.

The peak current (I_p) was initially varied through the gradual increase of the applied internal DC voltage (DC_{int}) while maintaining the generated film thickness at approximately 1.2 – 1.4 µm. This regime aims to identify the optimum deposition parameters that will generate dense films with better morphological properties. Selection details in series I will be further discussed in section 4.4.1. The Cr film deposited using the highest I_p was selected to be used in the second series where film thicknesses were varied by controlling the deposition time. Series II also shows that increasing the deposition time twice comparatively doubles the resulting film thickness, without making any changes to the other deposition parameters.

Table 1. Deposition parameters for the Cr films deposited by HiPIMS.

Series	V_p (V)	I_p (A)	P_p (kW)	F (Hz)	DC_{int} (V)	t_{dep} (min)	Thickness (µm)
I. Varying P_p *(at Low thickness)*	1065	44	47	207	300	25	1.4
	1226	54	66	150	350	30	1.4
	1400	63	90	112	400	35	1.4
	1374	94	133	113	400	40	1.2
II. Varying Thickness *(at High P_p)*	1399	95	134	113	400	90	2.5
	1398	94	133	113	400	180	5.4
	1417	96	138	113	400	360	10.3

The deposition rates for both series performed are shown in Fig. 4.1. Doubling the value of I_p resulted to a loss in deposition rate of about 50%. Several factors can be associated in the decrease of deposition rate as discussed in section 2.4.3. Two aspects that can greatly

attribute to this loss are the return and yield effects which results from back-attraction of sputtered atoms after ionization and sub-linear energy dependence of the sputtering yield, respectively. Both factors contribute to the decrease of deposition rate and can be related to the increase of I_p and V_p. This result is comparable with the data obtained by Samuelsson et al. [75] for Cr films obtained by HiPIMS having a reported loss of deposition rate close to 50% as well. Meanwhile, results in series II show that increasing the film thickness up to 10 times did not have any substantial effect on the deposition rate which consistently remained to be around 0.03 µm/min.

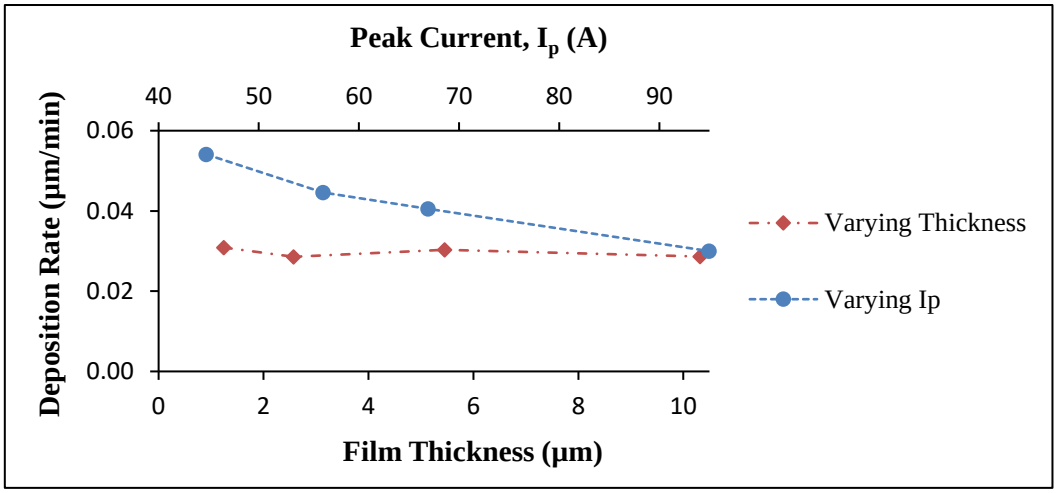

Figure 4.1. Deposition rate of Cr films deposited by HiPIMS as a function of peak current (I_p) and film thickness.

4.2 HiPIMS Discharge Characteristics

The behavior of V_p and I_p as a function of DC_{int} is depicted in Fig. 4.2. A linear increase of both V_p and I_p parameters is observed signifying a complementary increase of the ionization fraction of the sputtered species with the applied voltage.

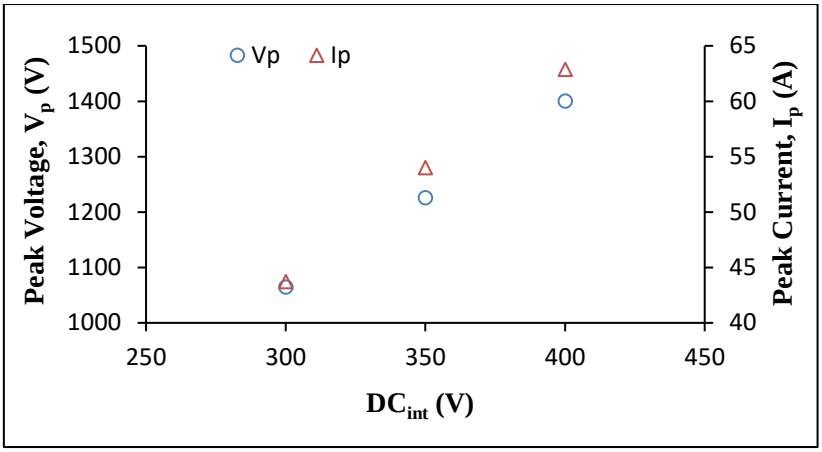

Figure 4.2. Evolution of peak voltage (V_p) and peak current (I_p) as a function of the charging voltage (DC_{int}).

The relationship of current (I) and voltage (V) in a magnetron plasma is found to obey the empirical power law $I \propto V^n$ having a typical value of exponent n ranging from 5 to 15 [76]. As shown in Fig. 4.3(a), the I-V characteristics of DCMS discharge was compared with HiPIMS based on previous work by Ferreira et. Al. [68] obtaining values of n at 12.5 and 2.7, respectively. The resulting low values of n are said to reflect the efficient ionization of discharge which is a typical occurrence for HiPIMS [61,77-78]. The calculated n values in this work are found to be even lower as shown in Fig. 4.3(b) indicating that further increase of voltage has a very minimal impact in the current, making the discharge ionization to be in an optimum condition.

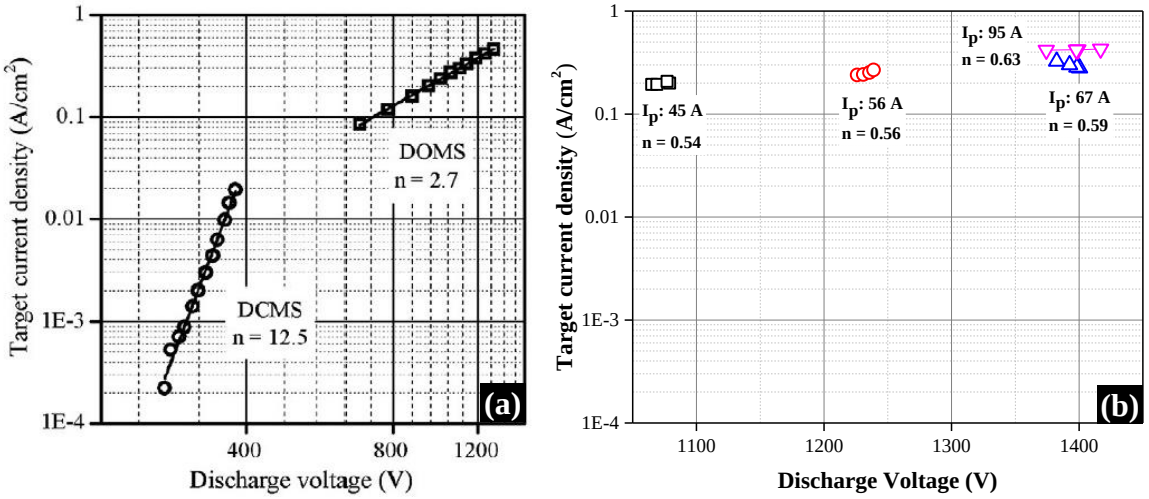

Figure 4.3. I-V characteristics from (a) reference work by Ferreira et al. [68], and (b) this research work using the maximum I_p and V_p of each pulse.

4.3 Film Morphology

4.3.1. Varying Peak Current

The cross-sectional SEM micrographs of deposited Cr films using series I of Table 1 at varying I_p are illustrated in Fig. 4.4 at a constant thickness of approximately 1.2 – 1.4 µm. Significant changes in film characteristics can be observed showing a shift from columnar to dense morphology as the values of I_p increased from 44 A up to 94 A. The columns extended from the substrate region up to the top surface of the film. Moreover, the columnar features are also evidently detected especially at the lowest I_p (Fig. 4.4a) near the substrate. These features become hardly distinguished in the Cr film with the highest I_p (Fig. 4.4d) with a more compact and dense morphology and only few traces of columnar remaining.

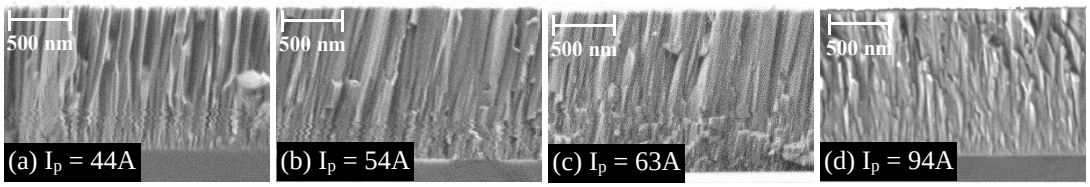

Figure 4.4. Cross-sectional SEM micrographs of the ~1-µm Cr films deposited by HiPIMS at different I_p: (a) 44 A, (b) 54 A, (c) 63 A and (d) 94 A.

These results confirmed the data trend from reference work [68] which also showed a significant transformation of columnar morphology to denser Cr film as the peak power, proportional to peak current, increases. Due to the generation of highly energetic ions, the deposition of denser films with less columnar microstructures in HiPIMS have been reported in several publications which in turn enhances the film properties [52,56,68]. In alignment of this research work's objective that is to deposit thick films with high density and good properties, further film analysis using other characterization techniques and material testing will be carried out using the deposited films of series II (I_p of 94 A at varying film thicknesses).

4.3.2. Varying Film Thickness

Figure 4.5 shows the cross-sectional SEM micrographs at 50,000x magnification of deposited films using series II of Table 1, maintaining the same deposition parameters except for the deposition time that was doubled per sample leading to films with thicknesses that

increased two times from previous. The micrographs are subdivided vertically per sample based on the resulting film thickness, and horizontally showing sequentially four different regions of film growth from the substrate to the top surface of 1.2, 2.5, 5, and 10 µm, respectively.

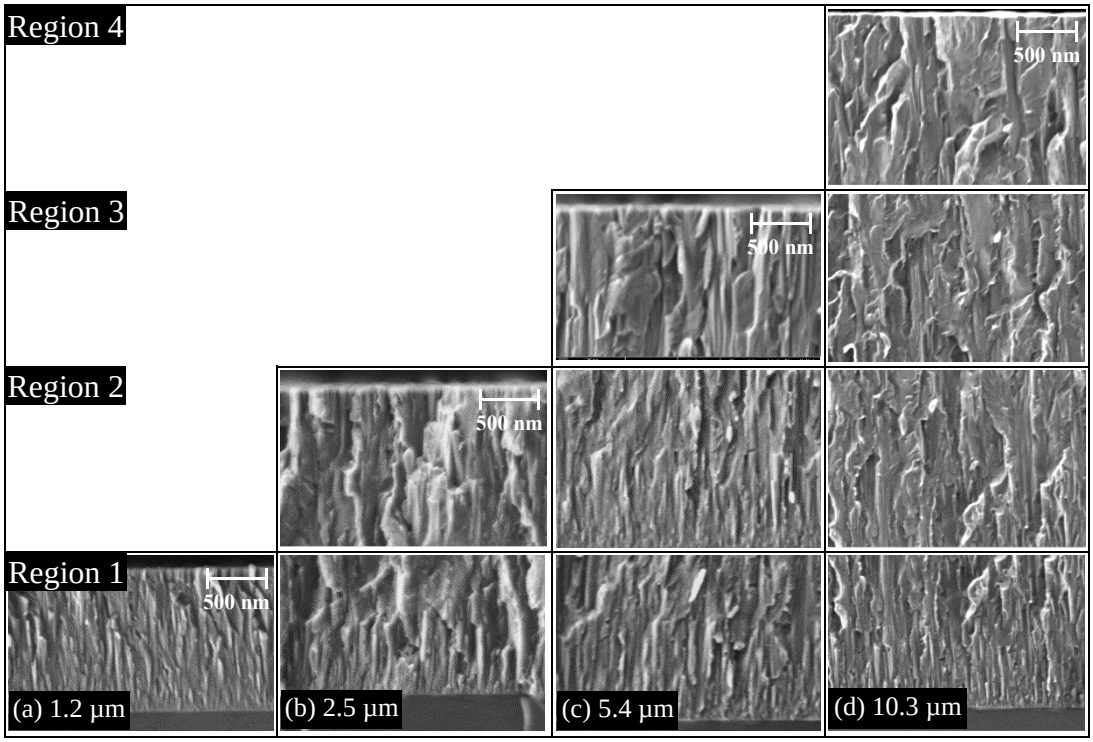

Figure 4.5. Cross-sectional SEM micrographs of the Cr films deposited by HiPIMS, subdivided (I) vertically at different thicknesses: (a) 1.2 µm, (b) 2.5 µm, (c) 5.4 µm and (d) 10.3 µm; and (II) horizontally at different regions: (1) substrate to 1.2-µm, (2) 1.2 to 2.5-µm, (3) 2.5 to 5.4-µm and (4) 5.4 to 10.3-µm section of thickness.

The generated films across all regions exhibited similar structure, although not featureless, yet still dense and compact especially when compared to the film morphology of the lower I_p values in Fig. 4.4. Similar observations have been reported to 1-µm Cr film deposited at high peak current at 98 A [68] and 10-µm CrN film deposited at 83 A [79]. Meanwhile, traces of short and disordered columnar grain growth can be noticed at Region 1 near the substrate for all film thicknesses. Such morphology is commonly evident to films at lower peak current as well as on coatings deposited using DC and pulsed DC magnetron sputtering [68]. There are no other significant differences between each region as the film growth progresses until the highest recorded film thickness. This confirms that the ideal dense and compact morphologies of Cr films have been maintained given the applied deposition parameters up to 10 µm.

4.4 Film Microstructure

4.4.1. XRD

The diffractograms of all Cr films deposited at various thicknesses have two dominant diffraction peaks that are indexed to (110) and (220) families of planes of BCC Cr crystalline structure as shown in Fig. 4.6. As the film thickness increases, no significant peak shifting has been identified on the XRD patterns indicating that the structure of deposited films is kept consistent irrespective of film thickness. The result supports the findings from SEM micrographs in Fig. 4.5 that also shows no distinct difference on the film morphology for each region of the developed film thicknesses.

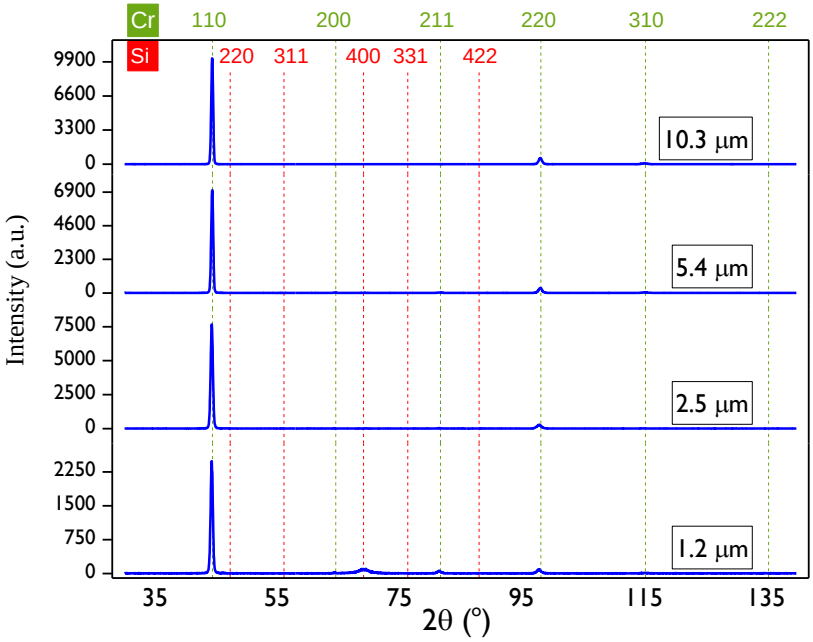

Figure 4.6. Diffractograms of the Cr films at different film thicknesses. Position of peaks from the powder ICDD card numbers 00-006-0694 of Cr and 00-027-1402 for Si are shown in green and red dotted lines, respectively, for reference on peak shifting.

Further evaluation of the preferred orientation of Cr films was performed using the obtained XRD patterns from θ–2θ configuration. The generated peak intensities from each pattern were then divided by the relative intensities from powder ICDD card of Cr resulting to the measured relative intensities of (110) and (220) shown in Fig. 4.7. Resulting value of 1 from the figure below indicates orientation similar to Cr standard, while values higher than 1

mean preferred orientation. All films clearly show a complete [110] orientation irrespective of the thicknesses indicating that all the grains contributing to X-ray diffraction in these films are orientated with their (110) planes parallel to the substrate. Meanwhile, random orientation was observed for (220) peak as values move closer to 1 with increasing film thickness.

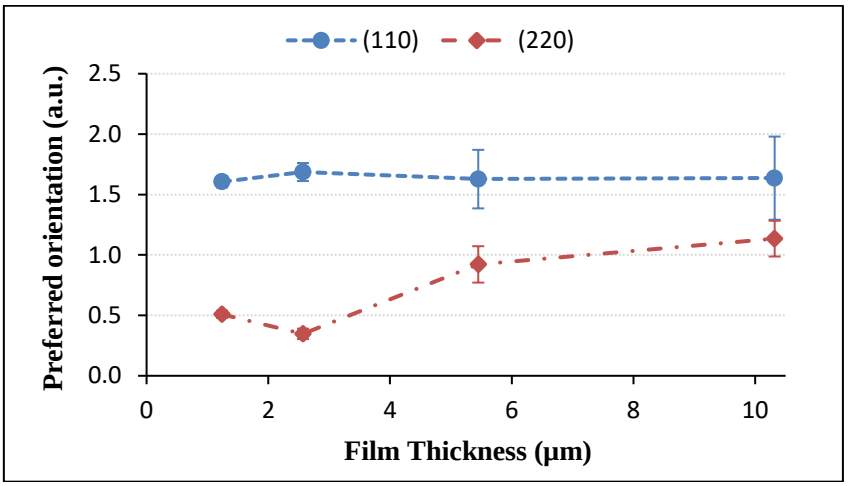

Figure 4.7. Evolution of the preferred orientation of (110) and (220) peaks from the deposited Cr films by HiPIMS at different film thicknesses.

Few traces of (211) diffraction peaks have also been detected from the Cr films with lower thicknesses although they are at very low intensity with only less than 1% compared to 85% relative intensity of (110) diffraction peak. Appearance of [111] preferred orientation is commonly associated to shadowing effect as the particles deposit at oblique angles forming columnar structure and rough surfaces [65]. The hints of (211) diffraction peaks can then be correlated to the observed short columnar residues in SEM micrographs (Fig. 4.5, Region 1), but the low intensity signifies the efficient prevention of shadowing effect through the deposition at high peak current which also contributed to the increased energy of bombarding particles.

The calculated lattice parameter $a_{(110)}$ and grain size from XRD spectra of Cr films in Fig. 4.6 have opposite trends with increasing film thickness as illustrated in Fig. 4.8. As the film thickness approaches to 10 µm, resulting values of lattice parameter $a_{(110)}$ decreases getting closer to the reported value of unstrained standard Cr (0.2284 nm as per ICDD card n◦ 00-006-0694), while the grain size significantly increases from 17 nm to 29 nm.

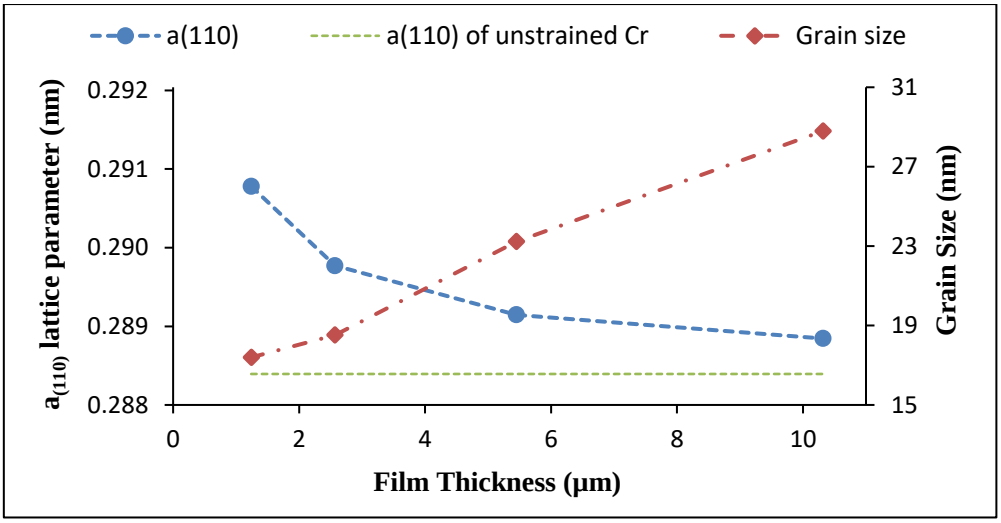

Figure 4.8. Effect of varying thicknesses on the lattice parameter (dashed line of unstrained Cr is added for reference), and average grain size of the Cr films deposited by HiPIMS.

The results of 1-µm film thickness are almost similar using the same deposition parameters with Ferreira et al. [68] indicating the formation of compressive stresses as a result of deposition at high peak power. However, the $a_{(110)}$ trend became completely opposite at increasing thickness versus analysis at increasing peak power (P_p) in [68], which may signify that further development of compressive stresses was avoided in spite of continuous bombardment with Cr ions as the film grows thicker. A minimal decrease on lattice parameters was also observed showing a small difference from 0.291 nm to 0.289 nm. Meanwhile, the increase of grain size is similar for film thicknesses beyond 5 µm in the study by Lin et al. [79] on CrN films using MPPMS. This occurrence may be associated to several factors such as compressive stresses, atomic shadowing, or formation of dislocations during film growth which will be discussed in detail on the next sections related to mechanical film properties.

4.4.2. Compressive Stress

One of the general sources of residual stresses in vacuum-based coatings such as in magnetron sputtering is intrinsic stress that develops due to the accumulation of crystallographic flaws during film deposition [80]. The intrinsic stress in sputtered films can also be related to the ESZM (Fig. 2.4) where films categorized under higher density zones, such as the deposited films in this work, often result to compressive stress in the coating due to argon entrapment and atomic peening from high energy bombardment [81]. As shown in Fig. 4.9, the results coincide with the ESZM as it exhibits an average compressive stress value

of -0.45 GPa. Comparable stress values were reported in previous study [82] of Cr film using hot target magnetron sputtering with thicknesses below 5 µm. Meanwhile, the recorded stress values for thick CrN films (> 5 µm) deposited by MPPMS [79] is more negative than the results in this work due to the reactive sputtering conditions (addition of Nitrogen) that increase bombardment during film growth.

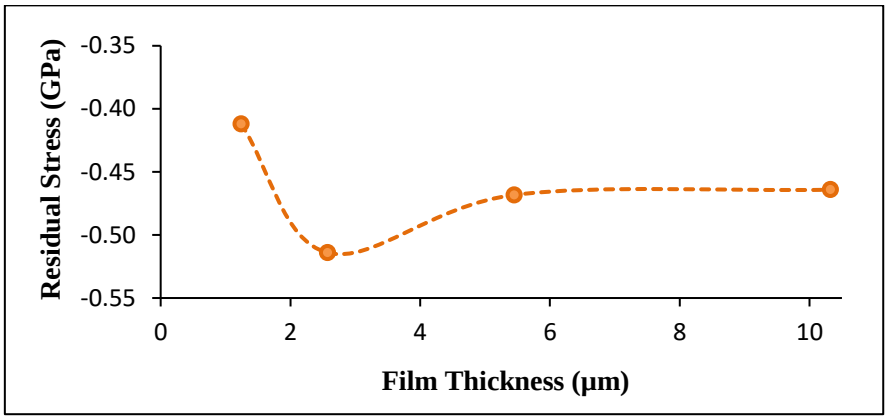

Figure 4.9. Dependence of the residual stresses of HiPIMS-deposited Cr coating on film thickness.

It can also be observed that the calculated residual stresses did not greatly vary with film thickness which can be accounted to relaxed momentum transfer at high ionization. Film growth involves longer deposition times and increased substrate temperature allowing more time for defects and dislocations to properly diffuse through crystalline structure and reach the grain boundaries where they are both absorbed and annihilated to release stress [83]. The constant trend of residual stresses with increasing thickness also supports the XRD results showing no significant shift of diffractions peaks and minimal change of lattice parameter.

4.5 Surface Properties

The surface morphology and topography of Cr coatings at different thicknesses are presented in Fig. 4.10 based on the obtained SEM micrographs and AFM scans. Film surfaces appear to have isotropic morphology with dense and highly compacted features as shown in the SEM micrographs (Fig. 4.10a), similar to the deposited Cr films by Ferreira et al. [84] using HiPIMS at high P_p. As the film grows thicker, the laminated feature on grains that are grown in random directions became more visible, which can be accounted to the high ion flux

bombardment. The same surface features were observed in Cr films deposited via MPPMS [85] at film thickness higher than 5 µm. Moreover, surface characteristics from both SEM and AFM evidently illustrates grain growth at increasing film thickness, thus supporting the obtained trend of grain size in Fig. 4.8.

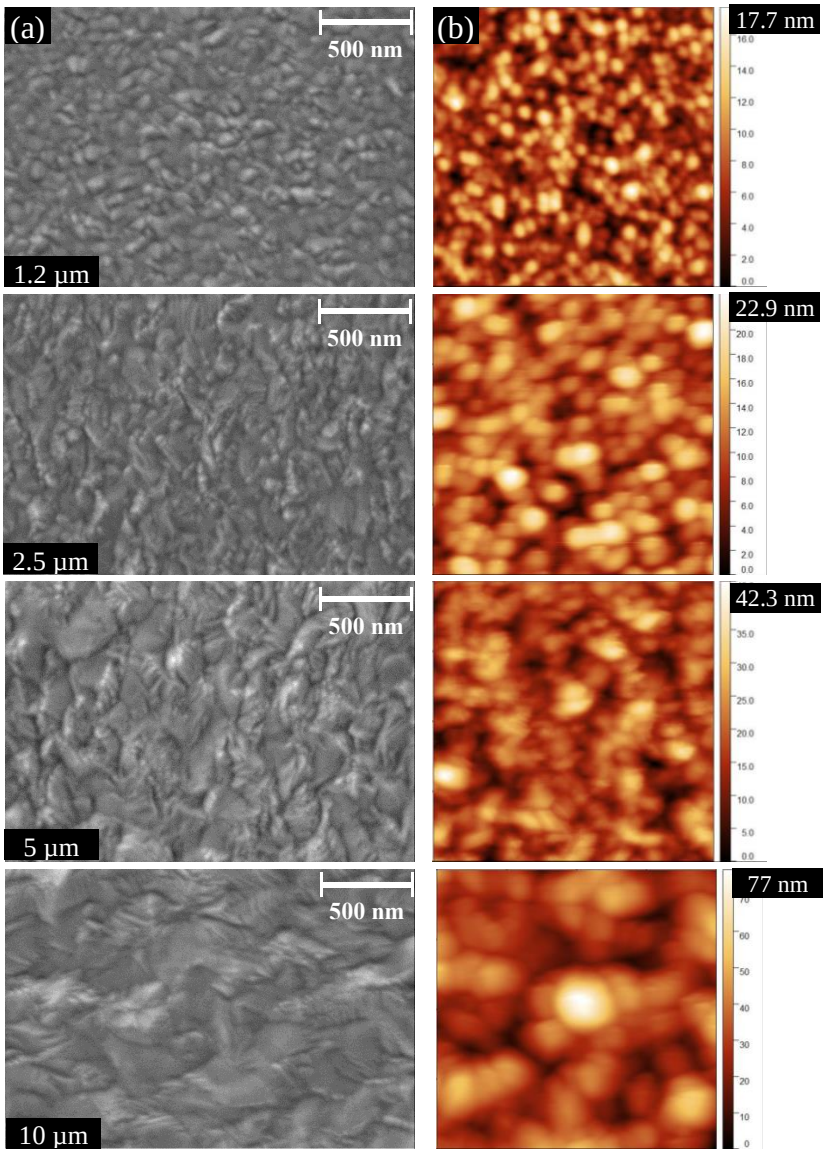

Figure 4.10. Surface morphology of Cr films deposited by HiPIMS as a function of film thickness: (a) SEM surface micrographs, and (b) representative AFM scans (2 × 2 µm).

The height of surface features (Rz) can also be compared from the labelled scale on the Z-axis of each AFM scan in Fig. 4.10b. As the Cr film grows thicker, Rz values also increase. This result can be correlated with the behavior of calculated surface roughness (Ra) from AFM scans.

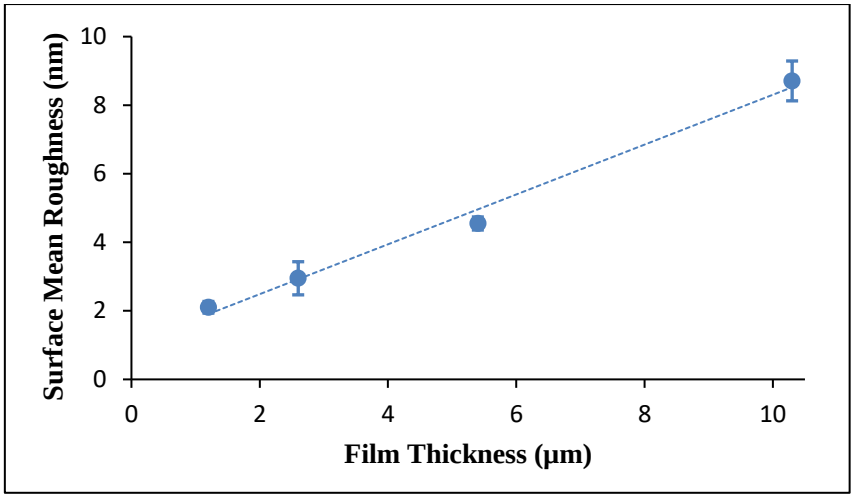

Figure 4.11. Surface mean roughness (Ra) calculated from the AFM scans of Cr films deposited by HiPIMS at varying film thickness.

The plotted Ra values in Fig. 4.11 as a function of film thickness illustrates an increasing trend, which can be linked with grain growth and the possible increase of macro particles in the surface. The calculated Ra values increased linearly with film thickness. Similar roughness values were obtained using the same deposition parameters for 1-um film deposited by HiPIMS [84] and 10-um film deposited by HPPMS with a hot target [71]. The increase in roughness is in accordance with Zone I features in ESZM (Fig. 2.4) demonstrating a "hit-and-stick" growth due to increase in flux density of deposited particles as film grows leading to rougher surfaces [70].

4.6 Mechanical Properties

4.6.1. Adhesive Strength

One of the commonly used testing methods to identify the adhesive strength of film coating is through scratch testing on one-side-coated samples like the deposited films in this work. The OM images of worn trails after scratch testing of Cr films at peak current of 94 A as a function of increasing thicknesses is illustrated in Fig. 4.12(a). The arrows indicate the subjectively determined critical load (L_c) at the start of coating delamination or onset of failure.

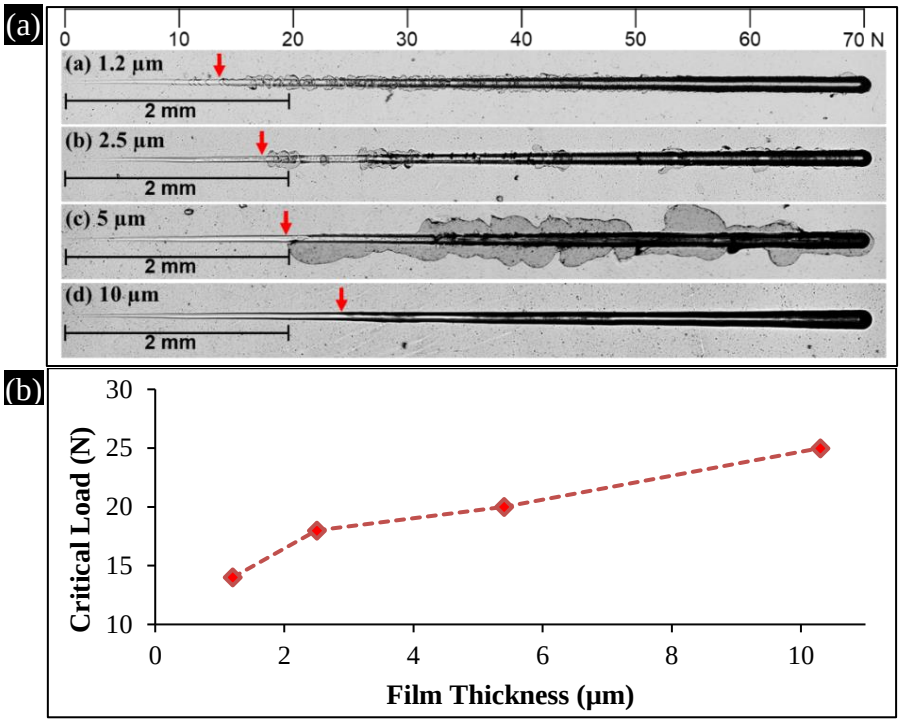

Figure 4.12. Results of the instrumented linear scratch testing of Cr films as a function of film thickness: (a) optical microscopy images of worn trails, (b) evolution of identified critical load for film delamination at variable deposited thicknesses (dashed line is a only a guide for the eyes).

Some cohesive spallation along the scratch track borders can be observed in films with thicknesses 1.2 µm and 2.5 µm, while large area interfacial spallation is noticeable in 5-µm Cr film. The thickest deposited film at 10 µm, on the other hand, only exhibited some Hertzian cracks within the scratch track without signs of delamination or spallation. Comparable image result of 10 µm was recorded in the developed 27-µm Cr film by Chen et. al. [86] via RFMS where authors suggested that such coatings have good adhesion and good deposition quality. This observation can be supported by the general trend of L_c values, as shown in Fig. 4.12(b), which increases from 15 N to 25 N as Cr film grows 10 times thicker from 1.2 µm. The measured L_c (27 N) in a 5-µm CrN deposited by MPPMS [79] is almost equivalent to the 10-µm film in this work considering that only pure Cr was utilized in this research. Several previous studies on various metallic coatings have reported the same effect of coating thickness on the scratch test critical load [86,87] showing that thicker Cr coatings are more capable of distributing the applied force as compared to the thinner films.

The mode of coating failure can also be associated to the intrinsic stresses in the film. Manifestation of spallation can be driven by residual compressive stress as analyzed in related studies [83,88] showing the occurrence of coating failure resulting from crack growth

at the substrate interface when some critical value of compressive stress is reached. Association of L_c with compressive stress can be further supported by the deposited pure Cr film using RFMS [89] that resulted to a critical value of 17 N as the films reached a constant compressive stress of -0.7 GPa. Such values are relatively similar in this work where the average compressive stress was at -0.5 GPa at L_c of 18 N.

4.6.2. Hardness and Toughness

The effect of increasing film thickness with hardness and elastic modulus are contrasting as shown in Fig. 4.13. The hardness of deposited films with low thicknesses (16 GPa) is closely comparable with the films deposited via HiPIMS at the same peak current having a recorded hardness of 17.7 GPa [68] showing reproducibility of films with high hardness. Meanwhile, the resulting hardness of 10.6 GPa for the thickest film (10 µm) in this work is still higher than the reported hardness values of 9.5 GPa and 8.2 GPa by Lin et al. [85] for MPPMS deposited 2.7-µm film and by Chen et al. [86] for RFMS deposited 27-µm film with -150 V bias, respectively. This clearly supports the effectivity of ionization by HiPIMS maintaining the high density of Cr film which then keeps the film hardness even without substrate biasing.

A gradual decrease in the coating hardness is also observed as film thickness increases showing the same trend with other related studies [79,82] using different magnetron sputtering techniques. One of the widely known factor attributed to hardness reduction is the Hall-Petch effect wherein nanocrystalline films have higher yield strength and hardness at some critical grain size (10-15 nm) [90]. Beyond such point, the grain boundaries act as barriers for the dislocations to glide along slip planes resulting to the accumulation of defects and absorption of residual stress on grain boundaries then leading to the decrease of film hardness [91]. As shown in Fig. 4.8, the calculated grain size for 1-µm film thickness is at 17 nm which is already beyond the identified critical grain size thus causing the decrease of hardness as thickness increases.

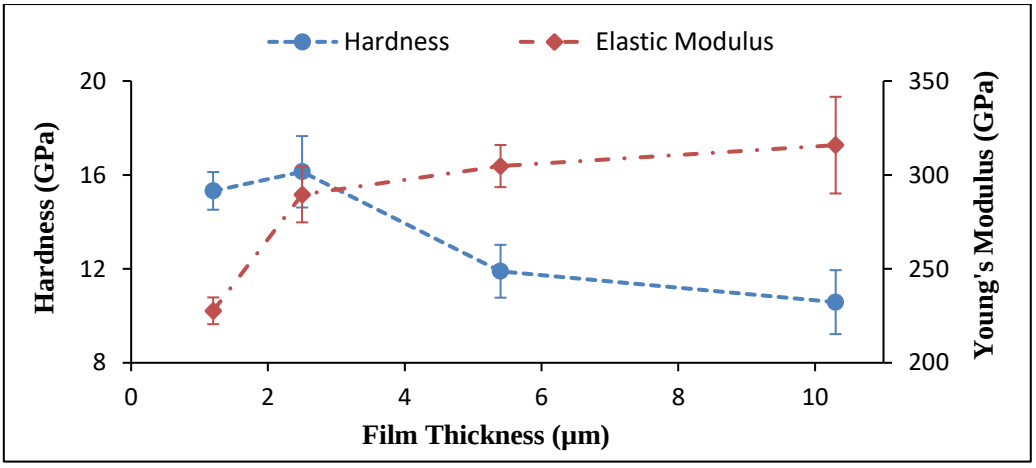

Figure 4.13. Hardness and Young's modulus of the Cr films deposited by HiPIMS.

The obtained Young's Modulus for the 1-µm film is almost the same as with the recorded value of the same thickness using DCMS [68]. Such low value of modulus had been accounted to the presence of porosity which is a typical characteristic on films deposited by DCMS. However, considering that Cr films deposited by HiPIMS are non-porous, dense, and compact as shown in Fig. 4.5, resistance against elastic deformation may have been influenced by the substrate material as evidently shown on the low value of modulus for the thinnest film. Since modulus corresponds to film elasticity in terms of the applied load, the distance from the point of test (film surface) to the substrate material has a great impact on the obtained results. Hence, as film thickness increases, the tendency of substrate influence decreases thus resulting to an increase of modulus from 2.5 µm to 10.3 µm films, with values higher than the bulk material (279 GPa). Moreover, modulus result of 10-µm film is comparable with the recorded data of 319 GPa for the 27-µm Cr film using RFMS [86] which further supports the high quality of film deposited by HiPIMS. The increasing trend of Young's Modulus can also be associated to the rise of critical load (Fig. 4.12b) signifying an improvement on the delamination behavior of coating as supported by similar study on scratch adhesion testing [87].

Meanwhile, the ratio of hardness to Young's Modulus (H/E) is found to be related with film toughness, implying that high ratio shows longer elastic strain to failure causes the film failure to be delayed as the material allows load redistribution over a large area [92]. A gradual drop of half the H/E ratio from 1-µm to 10-µm is shown in Fig. 4.14 which is predominantly determined by the reduction of film hardness as film thickness increases. Although the Young's Modulus of 1-µm film has much lower value than the bulk material, the calculated H/E ratio still has similar result as with previous study [68] having the same

deposition parameters in HiPIMS. Moreover, the exhibited H/E ratio of 0.034 for the 10-µm film in this work was found to be higher than the 9-µm film deposited by HPPMS [71] with H/E ratio of 0.02, indicating that the HiPIMS also develops tougher films.

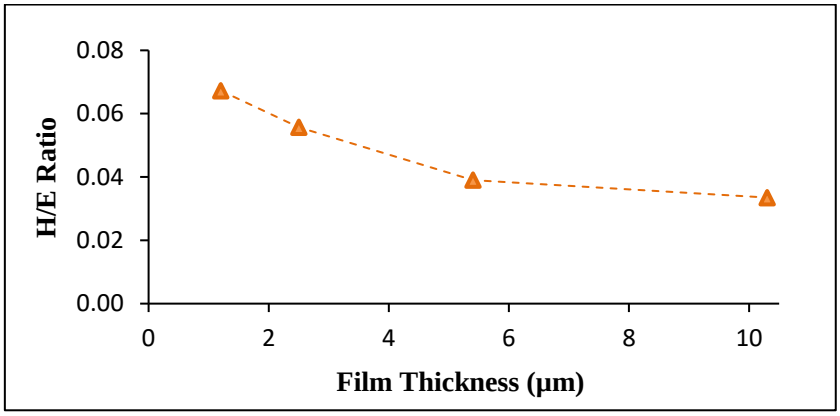

Figure 4.14. The H/E ratios of deposited Cr films at increasing film thickness.

4.7 Tribological Properties

Friction and wear behavior of the deposited Cr films on metal substrates were investigated using a pin-on-disc system. The measured COF for all films within the steady state regime (0.83 to 0.85) is typical for unlubricated steel-steel sliding contact [93]. The results exhibit an increase of COF in the first two thicknesses, but the difference is only 0.02% making the change generally insignificant as film thickness increases.

The measured wear rates on both the disc (where Cr film is deposited) and pin (steel ball) are also exhibited in Fig. 4.15. From thickness 1.2 µm to 2.5 µm, wear rates on both pin and disc significantly dropped to almost 90%, while trends going to 10-µm Cr film are opposite showing gradual decrease of less than 1% difference for disc wear rate, and around 5% increase for pin wear rate. Similar disc wear rate value of 0.37 x 10^{-6} mm^3/Nm was recorded on the same thickness (10 µm) of CrN film deposited by MPPMS [79] considering that the target material in this work only utilized a pure Cr without interlayer. Reduction of film wear rate can be attributed to the improved load carrying capacity and the increased scratch critical load (Fig. 4.12b) as the coating thickness was increased.

Meanwhile, the increase of wear rate on the ball can be accounted to film roughness showing the same trend in Fig. 4.11. Surfaces with high roughness have more asperities causing friction losses and consequently reflects to an increase in wear rate. The relationship of surface roughness on specific wear rate is supported in various related studies on metallic coatings [94-96].

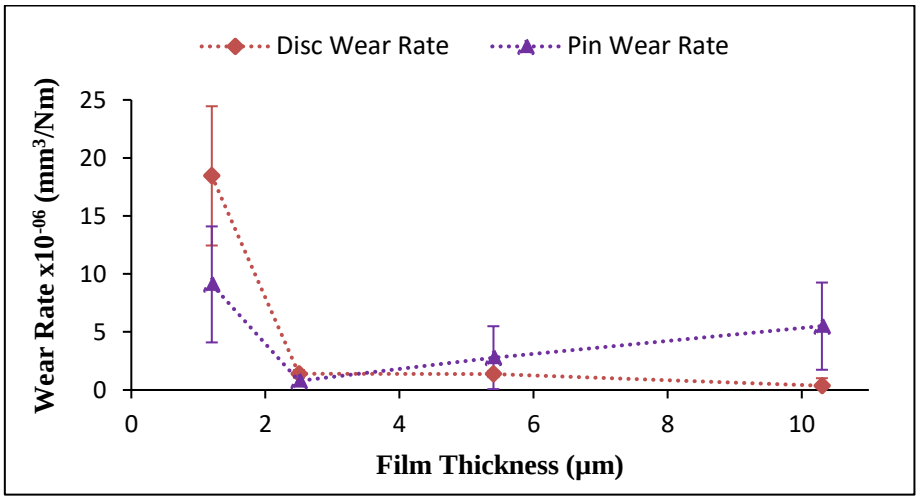

Figure 4.15. Coefficient of friction and wear rates on pin and disc of the Cr films deposited HiPIMS at different film thicknesses.

However, there are only limited tribological studies on vapor deposited Cr-based coatings, most of which are doped with interlayer(s) for property improvement, hence the obtained results cannot be vastly compared with other parameters specifically on pure Cr material. Nonetheless, the obtained wear rates in the Cr films deposited in this work are significantly lower than the calculated results on hard chrome plated coating having a wear rate value of 30 x 10^{-6} mm^3/Nm and above [97,98].

This signifies that the deposited Cr films using HiPIMS demonstrates an improved wear resistance as the film grows thicker which can be associated not only with the adhesive film strength, but also on the dense microstructure, and increased Young's Modulus that balances the hardness values indicating optimization of film toughness [99]. Moreover, the difference in wear rate behavior shows that wear is a property of the system, and not of the material. Results also indicate that the material wear rate depends on the interfacial conditions such as load carrying capacity and surface roughness of sliding surfaces.

5. CONCLUSION

5.1 Summary

The main objectives of the present work were achieved by depositing a dense Cr film with thickness above 1 μm using HiPIMS and understanding the effect of film growth on the surface and mechanical properties. To ensure that the deposited film is dense and compact, the first series of Cr films were deposited with increasing I_p at a constant thickness of 1 μm. Although the deposition rate decreased by 50% as I_p increases, the deposited film at the highest I_p (94 A) was found to be most dense with only few traces of columnar microstructure. Hence, the second series of Cr films was utilized with a constant I_p of 94 A, at increasing deposition time. Results showed that the thickness of deposited films doubled with deposition time until it reached to 10.3 μm after 360 minutes.

The dense and compact morphology of Cr films was maintained between each region, from the surface of 1-μm up to the 10-μm film, which agrees well with the crystalline structure having a [110] preferential orientation and no significant shift of peaks. All deposited films also exhibited compressive residual stress which evidently reflected on the high lattice parameter for 1-μm film. However, both the residual stresses and lattice parameter gradually decreased (or remained almost constant) as film thickness increases signifying the avoidance of further stress development due to relaxed momentum transfer at high ionization. Meanwhile, the calculated grain size increased with film thickness as projected in the obtained surface topography having more visible laminated features as grain grows at increasing thickness. Growth of grains influenced the increase in the height and roughness of film surface, and the decrease on film hardness.

The Cr films have demonstrated an improvement on delamination resistance showing enhancement of film adhesion. The increasing scratch test critical load as film thickness increases also show that thicker films are more capable of distributing the applied force. This consequently resulted to an increase in Young's Modulus and decrease of film wear rate signifying an improvement on elasticity and wear resistance, respectively. On the other

hand, the wear on the ball from the pin-on-disc test increased with thickness as a result of the increasing surface roughness. This shows that each film property has different effects on the investigated system.

Maintaining a dense tightly packed microstructure on the deposited films up to 10 μm shows the effectivity of high ionization in HiPIMS to prevent the shadowing effect, also avoiding the formation of defects and the development of compressive stresses. It can then be concluded that continuous bombardment of Cr^+ ions on growing film generally resulted to a change of film properties which can be mainly accounted to the increasing grain size and load carrying capacity as film thickness increases. These properties consequently had a gradual effect on other mechanical properties of films (hardness, toughness, wear rate) as supported by reference literatures.

5.2 Future Work

Effective deposition of highly dense and relatively thicker Cr film using HiPIMS allows more possibilities for future work to further improve the film properties. Using the parameters applied in this work, several aspects can be modified such as the deposition conditions and relevant testing. Application of bias in the deposition process can be explored to minimize surface roughness and enhance hardness. The corrosion resistance of PVD-coated Cr films may also be investigated as a function of increasing film thickness. Further evaluation of film composition can also be added using other characterization techniques (XPS, TEM, etc.) in order to identify the presence of oxides and other contaminants that may have affected the film properties.

The thick Cr film can also be utilized as a base layer for multilayered coatings. Reactive sputtering may be performed through the incorporation of interlayers on the deposited Cr films to strengthen the adhesive properties. In such manner, applicability of the developed film can reach a wider industry scope. Evaluation of films, like in tribological test, can then be further enhanced by using parameters that are closer to real operation conditions (e.g., high temperature, high load, extended test duration). More so, additional improvement on deposition technique and corresponding parameters can be investigated to obtain lesser deposition time on thicker films for it to be more cost efficient especially in industrial applications.

BIBLIOGRAPHY

[1] P. L. Cavallotti, "Editorial," *Electrochimica Acta*, vol. 50, no. 23, pp. 4523-4524, 2005.

[2] W. R. Grove, "On the Electro-Chemical Polarity of Gases," *Phil. Trans. Royal Soc.*, vol. 142, pp. 87–101, 1852.

[3] J. Lin and I. Dahan, "Nanostructured chromium coatings with enhanced mechanical properties and corrosion resistance," *Surf. Coat. Technol.*, vol. 265, pp. 154–159, 2015.

[4] A. Liang, Y. Li, H. Liang, L. Ni, and J. Zhang, "A favorable chromium coating electrodeposited from Cr(III) electrolyte reveals anti-wear performance similar to conventional hard chromium," *Mater. Lett.*, vol. 189, pp. 221–224, 2017.

[5] C. Langer, W. Wendland, K. Honold, L. Schmidt, J.S. Gutmann, and M. Dornbusch, "Corrosion analysis of decorative microporous chromium plating systems in concentrated aqueous electrolytes," *Eng. Fail. Anal.*, vol. 91, pp. 255–274, 2018.

[6] H. G. Kim, I. H. Kim, Y. I. Jung, D. J. Park, J. Y. Park, and Y. H. Koo, "Adhesion property and high-temperature oxidation behavior of Cr-coated Zircaloy-4 cladding tube prepared by 3D laser coating," *J. Nucl. Mater.*, vol. 465, pp. 531–539, 2015.

[7] H. Y. Yang, R. Q. Zhang, X. M. Peng, and M. L. Wang, "Research progress regarding surface coating of zirconium alloy cladding," *Surf. Technol.*, vol.46, no.1, pp. 69–75, 2017.

[8] Y. Wang, W. Zhou, Q. Wen, X. Ruan, F. Luo, G. Bai, Y. Qing, D. Zhu, Z. Huang, Y. Zhang, T. Liu, and R. Li, "Behavior of plasma sprayed Cr coatings and FeCrAl coatings on Zr fuel cladding under loss-of-coolant accident conditions," *Surf. Coat. Technol.*, vol. 344, pp. 141–148, 2018.

[9] X. Hu, C. Dong, Q. Wang, B. Chen, H. Yang, T. Wei, R. Zhang, W. Gu, and D. Chen, "High temperature oxidation of thick Cr coating prepared by arc deposition for accident tolerant fuel claddings," *J. Nucl. Mater.*, vol. 519, pp. 145–156, 2019.

[10] X. H. Yan, J. S. Li, W. R. Zhang, and Y. Zhang, "A brief review of high-entropy films," *Mater. Chem. Phys.*, vol. 210, pp. 12–19, 2018.

[11] W. Zhang, R. Tang, Z. B. Yang, C. H. Liu, H. Chang, J. J. Yang, J. L. Liao, Y. Y. Yang, and N. Liu, "Preparation, structure, and properties of high-entropy alloy multilayer coatings for nuclear fuel cladding: a case study of AlCrMoNbZr/(AlCrMoNbZr)N," *J. Nucl. Mater.*, vol. 512, pp. 15–24, 2018.

[12] A. S. Penfold, "Magnetron sputtering," in *Handbook of Thin Film Process Technology*, vol. 1, D. A. Glocker and S. I. Shah, Eds. Oxfordshire: Taylor & Francis, 2002.

[13] U. Helmersson, M. Lattemann, J. Bohlmark, A.P. Ehiasarian, and J.T. Gudmundsson, "Ionized physical vapor deposition (IPVD): A review of technology and applications," *Thin Solid Films,* vol. 513, nos. 1-2, pp. 1-24, 2006.

[14] D. Christie, "Target material pathways model for high power pulsed magnetron sputtering," *J. Vac. Sci. Technol*. A, vol. 23, pp. 330-335, 2005.

[15] K. Sarakinos, J. Alami, and S. Konstantinidis, "High power pulsed magnetron sputtering: A review on scientific and engineering state of the art," *Surf. Coat. Technol.,* vol. 204, pp. 1661-1684, 2010.

[16] H. S. Kim, S. S. Oh, H. S. Ha, D. Youm, S. H. Moon, J. H. Kim, S. X. Dou, Y. U. Heo, S. H. Wee, and A. Goyal, "Ultra-high performance, high temperature superconducting wires via cost-effective, scalable, co-evaporation process," *Sci. Rep*., vol. 4, p. 4744, 2014.

[17] J. Y. Yu, S. W. Chung, and J. R. Heath, "Silicon nanowires: preparation, device fabrication, and transport properties," *J. Phys. Chem. B,* vol. 104, no. 118, pp. 64–70, 2000.

[18] Z. Cui, J. Rothman, M. Klaui, L. Lopez-Diaz, J. VazCand Bland, "Fabrication of magnetic rings for high density memory devices," *Microelectron. Eng*., vol. 61, no. 577, p. 83, 2002.

[19] L. Martinu, and D. Poitras, "Plasma deposition of optical films and coatings: a review," *J. Vac. Sci. Technol.,* vol. 18, no. 2619, p. 45, 2000.

[20] L. Donohue, W. D. Münz, D. Lewis, J. Cawley, T. Hurkmans, T. Trinh, I. Petrov, and I. Greene, "Large-scale fabrication of hard superlattice thin films by combined steered arc evaporation and unbalanced magnetron sputtering," *Surf. Coat. Technol.*, vol. 93, pp. 69–87, 1997.

[21] S. Ito, T. N. Murakami, P. Comte, P. Liska, C. Grätzel, M. K. Nazeeruddin, and M. Grätzel, "Fabrication of thin film dye sensitized solar cells with solar to electric power conversion efficiency over 10%," *Thin Solid Films,* vol. 516, no. 4613, p. 9, 2008.

[22] Y. S. Yoon, H. J. Jung, W. K. Choi, and S. J. Yoon, "Method for making electrical and electronic devices with vertically integrated and interconnected thin-film type battery," U.S. Patent 6,264,709 B1, 2001.

[23] S. O. Mbam, S. E. Nwonu, O. A. Orelaja, U. S. Nwigwe, and X. F. Gou, "Thin-film coating; historical evolution, conventional deposition technologies, stress-state micro/nanolevel measurement/models and prospects projection: a critical review," *Mater. Res. Express,* vol. 6, no. 122001, 2019.

[24] H. O. Pierson, "Handbook of Chemical Vapor Deposition: Principles, Technology and Applications," Norwich: William Andrew Publishers, 1999.

[25] A. Baptista, J. Porteiro, J. Míguez, and G. Pinto, "Sputtering Physical Vapour Deposition (PVD) Coatings: A Critical Review on Process Improvement and Market Trend Demands," *Coatings,* vol. 8, no. 402, 2018.

[26] A. Jilani, M. Abdel-wahab, and A. Hammad, "Advance Deposition Techniques for Thin Film and Coating," *Modern Technologies for Creating the Thin-film Systems and Coatings*, no.8, Mar.2017. [Online serial]. Available: https://www.intechopen.com/books/. [Accessed: 23 Nov. 2020].

[27] A. Tsuchiya, Y. Fujiwara, and S. Okumura, "Cutting Performance and Wear Characteristics of Chromium Nitride-Coated Tools," *Mokuzai Gakkaishi*, vol. 54, pp. 263-271, 2008.

[28] H. Scheerer, H. Hoche, E. Broszeit, B. Schramm, E. Abele, and C. Berger, "Effects of the chromium to aluminum content on the tribology in dry machining using (Cr,Al)N coated tools," *Surf. Coat. Technol.*, vol. 200, nos. 1–4, pp. 203-207, 2005.

[29] T. Gong, P. Yao, X. Zuo, Z. Zhang, Y. Xiao, L. Zhao, H. Zhou, M. Deng, Q. Wang, and A. Zhong, "Influence of WC carbide particle size on the microstructure and abrasive wear behavior of WC–10Co–4Cr coatings for aircraft landing gear," *Wear*, vols. 362–363, pp. 135-145, 2016.

[30] M. Drożdż, K. Kyzioł, and Z. Grzesik, "Chromium-based oxidation-resistant coatings for the protection of engine valves in automotive vehicles," *Materiali in tehnologije*, vol. 51, pp. 603-607, 2017.

[31] G. Li, P. Deshpande, J. H. Li, and R. Y. Lin, "Nano Cr Interlayered CrN Coatings on Steels," *Tsinghua Science & Technology*, vol. 10, no. 6, pp. 690-698, 2005.

[32] N. C. Chuang, J. T. Lin, K. M. Chang, T. M. Tsai, K. C. Chang, and C. W. Wu, "The Film Thickness Effect on Electrical Conduction Mechanisms and Characteristics of the Ni-Cr Thin Film Resistor," *IEEE Journal of the Electron Devices Society*, vol. 4, no. 6, p. 441-444, 2016.

[33] A. Majid, A. Dar, A. Nabi, A. Shakoor, N. Hassan, A. Junjua, and Z. Jianjun, "Optical, electronic and magnetic properties of Cr:GaN thin films," *Materials Chemistry and Physics*, vol. 136, pp. 809–815, 2012.

[34] Y. Zhao, L. Wei, P. Yi, and L. Peng, "Influence of Cr-C film composition on electrical and corrosion properties of 316L stainless steel as bipolar plates for PEMFCs," *International Journal of Hydrogen Energy*, vol. 41, no. 2, pp. 1142-1150, 2016.

[35] S. Chatterjee, "Chromium Toxicity and its Health Hazards," *International Journal of Advanced Research*, vol. 3, pp. 167-172, 2015.

[36] IARC Working Group on the Evaluation of Carcinogenic Risks to Humans, *Chromium, Nickel and Welding* (IARC Monographs on the Evaluation of Carcinogenic Risks to Humans, No. 49), Lyon (FR): International Agency for Research on Cancer, 1990. [Online]. Available: https://www.ncbi.nlm.nih.gov/books/NBK519250/. [Accessed: 29 Nov. 2020].

[37] Occupational Safety and Health Administration, "Chromium (VI)," *Occupational Safety and Health Administration*, CFR 1910.1026, n.d. [Online]. Available: https://www.osha.gov/laws-regs/regulations/standardnumber/1910/1910.1026. [Accessed: 29 Nov. 2020].

[38] The Council of the European Union, "European Directive 2011/65/EU on the restriction of the use of certain hazardous substances in electrical and electronic equipment," *Official Journal of European Union*, 2011. [Online]. Available: http://data.europa.eu/eli/dir/2011/65/oj. [Accessed: 29 Nov. 2020].

[39] The Council of the European Union, "Commission Regulation (EU) 2017/999 amending Annex XIV to Regulation (EC) No 1907/2006 of the European Parliament and of the Council concerning the Registration, Evaluation, Authorisation and Restriction of Chemicals (REACH)," *Official Journal of European Union*, 2017. [Online]. Available: http://data.europa.eu/eli/reg/2006/1907/oj. [Accessed: 29 Nov. 2020].

[40] R. V. Umretiya, B. Elward, D. Lee, M. Anderson, R. Rebak, and J. Rojas, "Mechanical and chemical properties of PVD and cold spray Cr-coatings on Zircaloy-4," *Journal of Nuclear Materials*, vol. 541, no. 152420, 2020.

[41] N. Espallargas, J. Berget, J.M. Guilemany, A.V. Benedetti, and P.H. Suegama, "Cr3C2–NiCr and WC–Ni thermal spray coatings as alternatives to hard chromium for erosion–corrosion resistance," *Surf. Coat. Technol.*, vol. 202, no. 8, pp. 1405-1417, 2008.

[42] A. Förg, M. Blum, A. Killinger, J. Nicolás, and R. Gadow, "Deposition of chromium oxide-chromium carbide coatings via high velocity suspension flame spraying (HVSFS)," *Surf. Coat. Technol.*, vol. 351, pp. 171-176, 2018.

[43] S. F. Wang, H. C. Lin, H. Y. Bor, Y. L. Tsai, and C. N. Wei, "Characterization of chromium thin films by sputter deposition," *Journal of Alloys and Compounds*, vol. 509, no. 41, pp. 10110–10114, 2011.

[44] D. Wei, F. Li, S. Li, S. Wang, F. Ding, T. Tian, P. Zhang, and Z. Yao, "Effect of Cr ion implantation on surface morphology, lattice deformation, nanomechanical and fatigue behavior of TC18 alloy," *Applied Surface Science*, vol. 506, no. 145023, 2020.

[45] H. Khani, and J.F. Brennecke, "Hard chromium composite electroplating on high-strength stainless steel from a Cr(III)-ionic liquid solution," *Electrochemistry Communications*, vol. 107, no. 106537, 2019.

[46] D. Depla, S. Mahieu, J. E. Greene, "Chapter 5 - Sputter Deposition Processes," in *Handbook of Deposition Technologies for Films and Coatings*, 3rd ed. New York: William Andrew Publishing, 2010, pp. 253-296.

[47] D. Lundin, N. Brenning, D. Jädernäs, P. Larsson, E. Wallin, M. Lattemann, M. A. Raadu, and U. Helmersson, "Transition between the discharge regimes of high power impulse magnetron sputtering and conventional direct current magnetron sputtering," *Plasma Sources Sci. Technol.*, vol. 18, no. 045008, 2009.

[48] S. Konstantinidis, J. P. Dauchot, M. Ganciu, and M. Hecq, "Transport of ionized metal atoms in high-power pulsed magnetron discharges assisted by inductively coupled plasma," *Appl. Phys. Lett.*, vol. 88, no. 021501, 2006.

[49] D. Lundin and K. Sarakinos, "An introduction to thin film processing using high-power impulse magnetron sputtering," *Journal of Materials Research*, vol. 27, no. 5, pp. 780-792, 2012.

[50] J. T. Gudmundsson, P. Sigurjonsson, P. Larsson, D. Lundin, and U. Helmersson, "On the electron energy in the high power impulse magnetron sputtering discharge," *Journal of Applied Physics*, vol. 105, no. 123302, 2009.

[51] D. Lundin, "The HiPIMS Process", PhD dissertation, Linköping University Electronic Press, Linköping, 2010.

[52] A. P. Ehiasarian, P.Eh. Hovsepian, L. Hultman, and U. Helmersson, "Comparison of Microstructure and Mechanical Properties of Chromium Nitride-Based Coatings Deposited by High Power Impulse Magnetron Sputtering and by the Combined Steered Cathodic arc/Unbalanced Magnetron Technique," *Thin Solid Films*, vol. 457, pp. 270-277, 2004.

[53] A. P. Ehiasarian, W.-D. Münz, L. Hultman, U.Helmersson, and I. Petrov, "High Power Pulsed Magnetron Sputtered CrNx Films," *Surf. Coat. Technol.*, vol. 163-164, pp. 267-272, 2003.

[54] J. Bohlmark, M. Lattemann, J. T. Gudmundsson, A. P. Ehiasarian, Y. Aranda Gonzalvo, N. Brenning, and U. Helmersson, "The ion energy distributions and ion flux composition from a high power impulse magnetron sputtering discharge," *Thin Solid Films*, vol. 515, pp. 1522-1526, 2006.

[55] F. Eriksson, N. Ghafoor, F. Schaefers, E. Gullikson, and J. Birch, "Interface engineering of short-period Ni/V multilayer X-ray mirrors," *Thin Solid Films*, vol. 500, pp. 84-95, 2006.

[56] J. Alami, P. O. Å. Persson, D. Music, J. T. Gudmundsson, J. Bohlmark, and U. Helmersson, "Ion-assisted physical vapor deposition for enhanced film properties on nonflat surfaces," *J. Vac. Sci. Technol. A*, vol. 23, p. 278, 2005.

[57] J. Bohlmark, M. Östbye, M. Lattemann, H. Ljungcrantz, T. Rosell, and U. Helmersson, "Guiding the deposition flux in an ionized magnetron discharge," *Thin Solid Films*, vol. 515, no. 4, pp. 1928-1931, 2006.

[58] J. Alami, P. Eklund, J. M. Andersson, M. Lattemann, E. Wallin, J. Bohlmark, P. Persson, and U. Helmersson, "Phase tailoring of Ta thin films by highly ionized pulsed magnetron sputtering," *Thin Solid Films*, vol. 515, no. 3434, 2007.

[59] S. Konstantinidis, J. P. Dauchot, and M. Hecq, "Titanium oxide thin films deposited by high-power impulse magnetron sputtering," *Thin Solid Films*, vol. 515, no. 1182, 2006.

[60] M. D. Wiggins, M. C. Nelson, and C. R. Aita, "Phase development in sputter deposited titanium dioxide," *J. Vac. Sci. Technol. A*, vol. 14, no. 772, 1996.

[61] J. Alami, K. Sarakinos, F. Uslu, and M. Wuttig, "On the relationship between the peak target current and the morphology of chromium nitride thin films deposited by reactive high power pulsed magnetron sputtering," *J. Phys. D*, vol. 42, no. 015304, 2009.

[62] J. Paulitsch, P. H. Mayrhofer, C. Mitterer, W-D. Münz, and M. Schenkel, “Mechanical and tribological properties of CrN coatings deposited by a simultaneous HIPIMS/UBMsputtering process, in Society of Vacuum Coaters 50th Annual Technical Conference Proceedings, April 28–May 3 (Louisville, KY, 2007), p. 150.

[63] D. Mattox, “Chapter 7 - Physical Sputtering and Sputter Deposition (Sputtering)” in *Handbook of Physical Vapor Deposition (PVD) Processing*, 2nd ed. New York: William Andrew Publishing, 2010, pp. 237-286.

[64] R. Karunasiri, R. Bruinsma, and J. Rudnick, "Thin-film growth and the shadow instability," *Physical Review Letters*, vol. 62, p. 788, 1989.

[65] J. C. Oliveira, F. Ferreira, A. Anders, and A. Cavaleiro, “Reduced atomic shadowing in HiPIMS: Role of the thermalized metal ions,” *Applied Surface Science*, vol. 433, pp. 934–944, 2018.

[66] F. Ferreira, “Process-properties relations in deep oscillation magnetron sputtering”, PhD thesis, University of Coimbra, Coimbra, 2018.

[67] V. Tiron, I.L. Velicu, O. Vasilovici, and G. Popa, “Optimization of deposition rate in HiPIMS by controlling the peak target current,” *J. Phys. D: Appl. Phys.*, vol. 48, no. 495204, 2015.

[68] F. Ferreira, R. Serra, J. Oliveira, and A. Cavaleiro, "Effect of peak target power on the properties of Cr thin films sputtered by HiPIMS in deep oscillation magnetron sputtering (DOMS) mode," *Surf. Coat. Technol.*, vol. 258, pp. 249-256, 2014.

[69] J. A. Thornton, “Influence of Apparatus Geometry and Deposition Conditions on the Structure and Topography of Thick Sputtered Coatings,” *J. Vac. Sci. Technol.*, vol. 11, pp. 666–670, 1974.

[70] S. Mahieu, P. Ghekiere, D. Depla, and R. De Gryse, “Biaxial alignment in sputter deposited thin films,” *Thin Solid Films*, vol. 515, no. 4, pp. 1229-1249, 2006.

[71] V. A. Grudinin, G. A. Bleykher, D. V. Sidelev, V. P. Krivobokov, M. Bestetti, A. Vicenzo, and S. Franz, “Chromium films deposition by hot target high power pulsed magnetron sputtering: Deposition conditions and film properties,” *Surf. Coat. Technol.*, vol. 375, pp. 352-362, 2019.

[72] A. De Monteynard, F. Schuster, A. Billard, and F. Sanchette, “Properties of chromium thin films deposited in a hollow cathode magnetron powered by pulsed DC or HiPIMS,” *Surf. Coat. Technol.*, vol. 330, pp. 241-248, 2017.

[73] G. G. Stoney, "The tensions of metallic films deposited by electrolysis," *Proc. R. Soc. Land. A*, vol. 82, pp. 172–175, 1909.

[74] J. F. Archard, "Contact and Rubbing of Flat Surfaces," *J. Appl. Phys.*, vol. 24, pp. 981–988, 1953.

[75] M. Samuelsson, D. Lundin, J. Jensen, M. A. Raadu, J. T. Gudmundsson, and U. Helmersson, "On the film density using high power impulse magnetron sputtering," *Surf. Coat. Technol.*, vol. 205, pp. 591–596, 2010.

[76] S. M. Rossnagel and H. R. Kaufman, "Current–voltage relations in magnetrons," *J. Vac. Sci. Technol. A*, vol. 6, pp. 223–229, 1988.

[77] F. Papa, H. Gerdes, R. Bandorf, A. P. Ehiasarian, I. Kolev, G. Braeuer, R. Tietema, and T. Krug, "Deposition rate characteristics for steady state high power impulse magnetron sputtering (HIPIMS) discharges generated with a modulated pulsed power (MPP) generator," *Thin Solid Films*, vol. 520, pp. 1559–1563, 2011.

[78] D. J. Christie, "Fundamentals of high power pulsed magnetron sputtering: Visualization of mechanisms for rate reduction and increased ion fraction," *Czechoslov. J. Phys.*, vol. 56, pp. B93–B97, 2006.

[79] J. Lin, W. D. Sproul, J. J. Moore, S. Lee, and S. Myers, "High rate deposition of thick CrN and Cr2N coatings using modulated pulse power (MPP) magnetron sputtering," *Surf. Coat. Technol.*, vol. 205, pp. 3226–3234, 2011.

[80] J. A. Thornton, "Stress-related effects in thin films," *Thin Solid Films*, vol. 171, pp. 5-31, 1989.

[81] H. Windischmann, "Intrinsic stress in sputter-deposited thin films," *Critical Reviews in Solid State and Material Sciences*, vol. 17, no. 6, pp. 547-596, 1992.

[82] D. V. Sidelev, M. Bestetti, G. A. Bleykher, V. P. Krivobokov, V. A. Grudinin, S. Franz, A. Vicenzo, and Y. L. Shanenkova, "Deposition of Cr films by hot target magnetron sputtering on biased substrates," *Surf. Coat. Technol.*, vol. 350, pp. 560-568, 2018.

[83] V. Teixeira, "Mechanical integrity in PVD coatings due to the presence of residual stresses," *Thin Solid Films*, vol. 392, pp. 276-281, 2001.

[84] F. Ferreira, R. Serra, A. Cavaleiro, and J. C. Oliveira, "Additional control of bombardment by deep oscillation magnetron sputtering: Effect on the microstructure and topography of Cr thin films," *Thin Solid Films*, vol. 619, pp. 250–260, 2016.

[85] J. Lin, J. J. Moore, W. D. Sproul, B. Mishra, and Z. Wu, "Modulated pulse power sputtered chromium coatings," *Thin Solid Films*, vol. 518, pp. 1566–1570, 2009.

[86] Q. S. Chen, C. H. Liu, R. Q. Zhang, H. Y. Yang, T. G. Wei, Y. Wang, Z. Li, L.X. He, J. Wang, L. Wang, J. P. Long, and H. Chang, "Microstructure and high-temperature steam oxidation properties of thick Cr coatings prepared by magnetron sputtering for accident tolerant fuel claddings: The role of bias in the deposition process," *Corrosion Science*, vol. 165, p. 108378, 2020.

[87] A. J. Perry, "Scratch adhesion testing of hard coatings," *Thin Solid Films*, vol. 107, pp. 167-180, 1983.

[88] S. J. Howard, Y. C. Tsui, and T. W. Clyne, "The effect of residual stresses on the debonding of coatings - I. A model for delamination at a bimaterial interface," *Acta Metall. Mater*., vol. 42, no. 8, pp. 2823-2836, 1994.

[89] V. Guilbaud-Massereau, A. Celerier, and J. Machet, "Study and improvement of the adhesion of chromium thin films deposited by magnetron sputtering," *Thin Solid Films*, vol. 258, pp. 185-193, 1995.

[90] T. G. Nieh and J. Wadsworth, "Hall-Petch relation on nanocrystalline solids," *Scr. Met. Mater*., vol. 25, pp. 955–958, 1991.

[91] T. Narutani and J. Takamura, "Grain-size strengthening in terms of dislocation density measured by resistivity," *Acta Metall. Mater*., vol. 39, pp. 2037–2049, 1991.

[92] J. Musil, "Hard nanocomposite coatings: thermal stability, oxidation resistance and toughness," *Surf. Coat. Technol.*, vol. 207, pp. 50–65, 2012.

[93] C. Rebholz, H. Ziegele, A. Leyland, and A. Matthews, "Structure, mechanical and tribological properties of nitrogen-containing chromium coatings prepared by reactive magnetron sputtering," *Surf. Coat. Technol.*, vol. 115, pp. 222–229, 1999.

[94] R. A. Al-Samarai, Haftirman, K. R. Ahmad, and Y. Al-Douri, "The Influence of Roughness on the Wear and Friction Coefficient under dry and lubricated sliding," *International Journal of Scientific and Engineering Research*, vol. 3, no. 4, 2012.

[95] R. A. Al-Samarai, Haftirman, K. R. Ahmad, and Y. Al-Douri, "Evaluate the Effects of Various Surface Roughness on the Tribological Characteristics under Dry and Lubricated Conditions for Al-Si Alloy," *Journal of Surface Engineered Materials and Advanced Technology*, vol. 2, pp. 167-173, 2012.

[96] D. H. Cho, S. A. Lee, and Y. Z. Lee, "The Effects of Surface Roughness and Coatings on the Tribological Behavior of the Surfaces of a Piston Skirt," *Tribology Transactions*, vol. 53, pp. 137-144, 2009.

[97] S. Mitrović, M. Babić, D. Adamović, F. Živić, D. Džunić, and M. Pantića, "Wear Behaviour of Hard Cr Coatings for Cold Forming Tools Under Dry Sliding Conditions," *Tribology in Industry*, vol. 34, no. 1, pp. 44-48, 2012.

[98] G. Bolelli, V. Cannillo, L. Lusvarghi, and S. Riccò, "Mechanical and tribological properties of electrolytic hard chrome and HVOF-sprayed coatings," *Surf. Coat. Technol.*, vol. 200, no. 9, pp. 2995-3009, 2006.

[99] A. Leyland and A. Matthews, "On the significance of the H/E ratio in wear control: a nanocomposite coating approach to optimised tribological behaviour," *Wear*, vol. 246, pp. 1–11, 2000.